SANDIA REPORT
SAND2010-5901
Unlimited Release
Printed September 2010

Development of a New Generation of Waste Form for Entrapment and Immobilization of Highly Volatile and Soluble Radionuclides

Yifeng Wang, Huizhen Gao, C. Jeffrey Brinker, Yongliang Xiong, Kathleen Holt, Andy Miller, Phillip Pohl, Nathan Ockwig, Mark A. Rodriquez, Denise N. Bencoe, Hernesto Tellez, Jessica Nicole Kruichak, Rigney Turnham, and Andrew Wilson Murphy

Prepared by
Sandia National Laboratories
Albuquerque, New Mexico 87185 and Livermore, California 94550

Sandia National Laboratories is a multi-program laboratory managed and operated by Sandia Corporation, a wholly owned subsidiary of Lockheed Martin Corporation, for the U.S. Department of Energy's National Nuclear Security Administration under contract DE-AC04-94AL85000.

Issued by Sandia National Laboratories, operated for the United States Department of Energy by Sandia Corporation.

Available to DOE and DOE contractors from
U.S. Department of Energy
Office of Scientific and Technical Information
P.O. Box 62
Oak Ridge, TN 37831

Telephone: (865) 576-8401
Facsimile: (865) 576-5728
E-Mail: reports@adonis.osti.gov
Online ordering: http://www.osti.gov/bridge

Available to the public from
U.S. Department of Commerce
National Technical Information Service
5285 Port Royal Rd.
Springfield, VA 22161

Telephone: (800) 553-6847
Facsimile: (703) 605-6900
E-Mail: orders@ntis.fedworld.gov
Online order: http://www.ntis.gov/help/ordermethods.asp?loc=7-4-0#online

SAND2010-5901
Unlimited Release
Printed September 2010

Development of a New Generation of Waste Form for Entrapment and Immobilization of Highly Volatile and Soluble Radionuclides

Yifeng Wang[1], Huizhen Gao[1], C. Jeffrey Brinker[2], Yongliang Xiong[3], Kathleen Holt-Larese[4], Andy Miller[1], Phillip Pohl[5], Nathan Ockwig[6], Mark A. Rodriquez[7], Denise N. Bencoe[8], Hernesto Tellez[1], Jessica Nicole Kruichak[1], Rigney Turnham[1], and Andrew Wilson Murphy[1]

[1]Radiological Consequence Management & Response Technologies Department
[2]Self-Assembled Materials Department
[3]Repository Performance Department
[4]Global Physical Security Program Department
[5]Risk & Reliability Analysis Department
[6]Geochemistry Department
[7]Materials Characterization Department
[8]Ceramic Processing Department

Sandia National Laboratories
P.O. Box 5800
Albuquerque, New Mexico 87185-MS0779

Abstract

The United States is now re-assessing its nuclear waste disposal policy and re-evaluating the option of moving away from the current once-through open fuel cycle to a closed fuel cycle. In a closed fuel cycle, used fuels will be reprocessed and useful components such as uranium or transuranics will be recovered for reuse. During this process, a variety of waste streams will be generated. Immobilizing these waste streams into appropriate waste forms for either interim storage or long-term disposal is technically challenging. Highly volatile or soluble radionuclides such as iodine (^{129}I) and technetium (^{99}Tc) are particularly problematic, because both have long half-lives and can exist as gaseous or anionic species that are highly soluble and poorly sorbed by natural materials. Under the support of Sandia National Laboratories (SNL) Laboratory-Directed Research & Development) (LDRD), we have developed a suite of inorganic nanocomposite materials (SNL-NCP) that can effectively entrap various radionuclides, especially for ^{129}I and ^{99}Tc. In particular, these materials have high sorption capabilities for iodine gas. After the sorption of radionuclides, these materials can be directly converted into nanostructured waste forms. This new generation of waste forms incorporates radionuclides as

nano-scale inclusions in a host matrix and thus effectively relaxes the constraint of crystal structure on waste loadings. Therefore, the new waste forms have an unprecedented flexibility to accommodate a wide range of radionuclides with high waste loadings and low leaching rates.

Specifically, we have developed a general route for synthesizing nanoporous metal oxides from inexpensive inorganic precursors. More than 300 materials have been synthesized and characterized with x-ray diffraction (XRD), BET surface area measurements, and transmission electron microscope (TEM). The sorption capabilities of the synthesized materials have been quantified by using stable isotopes I and Re as analogs to ^{129}I and ^{99}Tc. The results have confirmed our original finding that nanoporous Al oxide and its derivatives have high I sorption capabilities due to the combined effects of surface chemistry and nanopore confinement. We have developed a suite of techniques for the fixation of radionuclides in metal oxide nanopores. The key to this fixation is to chemically convert a target radionuclide into a less volatile or soluble form. We have developed a technique to convert a radionuclide-loaded nanoporous material into a durable glass-ceramic waste form through calcination. We have shown that mixing a radionuclide-loaded getter material with a Na-silicate solution can effectively seal the nanopores in the material, thus enhancing radionuclide retention during waste form formation. Our leaching tests have demonstrated the existence of an optimal vitrification temperature for the enhancement of waste form durability. Our work also indicates that silver may not be needed for I immobilization and encapsulation.

Acknowledgments

This work is supported by DOE Sandia Laboratory-Directed Research & Development (LDRD) Program and partly by DOE Fuel Cycle Research & Development (FCR&D) Program. We would like to thank Stephanie P. Kuzio, Kevin A. McMahon, and John E. Kelly for their management support and encouragement. We would also like to thank Dana A. Powers for his invaluable technical insights.

Contents

Figures

Tables

Nomenclature

BET	Brunauer, Emmett, and Teller
DOE	Department of Energy
EDXRF	Energy-Dispersive X-Ray Fluorescence
FTIR	Fourier Transformation Infrared spectroscopy
GCMC	Grand Canonical Monte Carlo
I	Iodine
Kr	Krypton
LDRD	Laboratory Directed Research & Development
SNL	Sandia National Laboratories
SNL-NCP	Sandia Developed Nanocomposite
TGA	Thermal gravimetric analyzer
TEM	Transmission Electron Microscope
Tc	Technetium
Xe	Xenon
XPS	X-ray photoelectron spectrum
XRD	X-Ray Diffractometer

1. Introduction

The United States is now re-assessing its nuclear waste disposal policy and re-evaluating the option of moving away from the current once-through open fuel cycle to a closed fuel cycle. In a closed fuel cycle, used fuels will be reprocessed and useful components such as uranium or transuranics will be recovered for reuse (e.g., Bodansky, 2006). During this process, a variety of waste streams will be generated (NEA, 2006; Gombert, 2007). Immobilizing these waste streams into appropriate waste forms for either interim storage or long-term disposal is technically challenging (Peters and Ewing, 2007; Gombert, 2007). Highly volatile or soluble radionuclides such as iodine (^{129}I) and technetium (^{99}Tc) are particularly problematic, because both have long half-lives and can exist as gaseous or anionic species that are highly soluble and poorly sorbed by natural materials (Wang et al., 2003; Wang and Gao, 2006; Wang et al., 2007). Waste forms are probably the only engineered barrier to limit their release into a human-accessible environment after disposal. In addition, during the fuel reprocessing, a major fraction of volatile radionuclides (e.g. >94% for ^{129}I) will enter the gas phase and must be captured in the off-gas treatment (see detailed discussion in the next section). It is thus highly desirable to develop a material that can effectively capture these radionuclides and then be converted into a durable waste form.

Under the support of Sandia National Laboratories (SNL) Laboratory-Directed Research & Development) (LDRD), we have developed a suite of inorganic nanocomposite materials (SNL-NCP) that can effectively entrap various radionuclides, specifically for ^{129}I and ^{99}Tc. Our testing data show that these materials have high sorption capabilities for iodine gas. Importantly, after the sorption of radionuclides, these materials can be converted into nanostructured waste forms, which are expected to have unprecedented flexibility to accommodate a wide range of radionuclides with high waste loadings and low leaching rates. In this document, we summarize the results of SNL-NCP material development and the performance of these materials.

2. Current Status of Off-Gas Treatment in Fuel Reprocessing

In fuel reprocessing, spent fuels are first subjected to voloxidation and acid dissolution, during which 94% to 99% of iodine-129, together with other volatile radionuclides (^{14}C, ^{3}H, Kr and Xe), are released to the off-gas stream (Gombert, 2007). Various methods have been proposed for the recovery of volatile ^{129}I, including scrubbing with caustic or acid solutions and chemisorption on impregnated adsorbents (Rovnyi et al., 2002; Kato et al., 2002; Gombert, 2007). The proposed adsorbents include both natural and artificial porous materials like zeolite (e.g., mordenite), alumina, and silica gels loaded with metals (e.g., Ag, Cd, Pb) that form low-solubility iodides or iodates. However, several issues have been recognized regarding the effectiveness of these materials (Gombert, 2007). For example, based on adsorption models, iodine diffusion inside the zeolite particles was found to be slow, only about 2×10^{-14} cm^2/s, and likely to limit the adsorption process (Jubin, 1994, Gombert, 2007). In addition, silver-exchanged faujasite (AgX) decomposes in the presence of NO_x and water vapor. AgX also does

not exhibit satisfactory thermal stability during regeneration. Silver-impregnated alumina and silica capture iodine by forming AgI along grain boundaries. The high iodine leaching rate of these materials can be a potential concern if they are directly used for disposal. Currently, no path forward has been established for the disposition of these adsorbent materials.

Entrapping noble gas radionuclides (Kr and Xe) in an off-gas stream is technically challenging, because they are chemically inert. Only a very aggressive agent such as fluorine gas can form compounds with them. Several methods have been proposed and studied for trapping radioactive noble gas stream from the off-gas in the reprocessing processes. These methods include cryogenic distillation, membrane separation, and adsorption to solid adsorbents. Cryogenic sequestration and storage in pressure containers have been proposed for interim disposal of radioactive xenon (Xe) and krypton (Kr). However, the cryogenic method suffers from drawbacks such as high operating costs and the potential for fire hazard due to ozone accumulation. The problem with a membrane separation process is the lower throughput. The adsorption process is a promising method because of its simplicity and reliability, relative to cryogenic distillation and membrane separation.

Selection of an appropriate adsorbent is key to the development of an adsorption process. Zeolite has been found to exhibit a relatively high loading for noble gases (Ianovski et al., 2002; Munakata et al., 2003; Webster et al., 1999). It has been shown that krypton can be encapsulated in the zeolite structure by a sintering process where micropores of the zeolite are sealed (Gombert, 2007). However, the usage of hydrogen and silver end-members of mordenite is not cost effective. In addition, the fibrous nature of mordenite may present an inhalation hazard (Stephenson et al., 1999) to the safety of operation workers. Exploratory operations of the adsorption process by using activated charcoal were conducted at some organizations because of the high adsorption capacities of these materials. However, further development of this technique was suspended due to the volatile reaction between NO_x and the activated charcoal, which could contribute to fire hazard.

Development and optimization of adsorbent materials for capture of radioactive noble gases require mechanistic understanding of the interaction of these gases with solid surfaces. Such information can be drawn from recent studies that use the stable isotope ^{129}Xe as a probing molecule to characterize porous materials (Terskikh et al., 1999; Hiejima et al., 2006). The adsorption of Xe onto zeolite or a nanostructured surface has been studied with Nuclear Magnetic Resonance (NMR) spectroscopy. The adsorption of a noble gas is attributed to van der Waals forces resulting from polarization of Xe molecule (Dil et al., 2008).

3. A New Paradigm for Waste Form Development: Nano-Scale Radionuclide Immobilization and Encapsulation

The development of SNL-NCP materials are based on the concept of nano-scale radionuclide immobilization and encapsulation (Figure 1). Using iodine as an example, a nanoporous material is engineered to have a high sorption capability for iodine gas. The pore

surface of the material is modified as needed to maximize this capability. The material is then used as an adsorbent to entrap gaseous iodine. The entrapped iodine is converted to a less volatile compound, for example, by reacting with silver to form AgI precipitates inside nanopores of the material. The idoine-loaded material is finally mixed with glass-forming constituents and calcined, resulting in a waste form in which I-bearing nanoparticles are embedded in a glass or crystalline matrix. More recent development of this technology allows us to avoid using Ag or other heavy metals for iodine immobilization and subsequent vitrification.

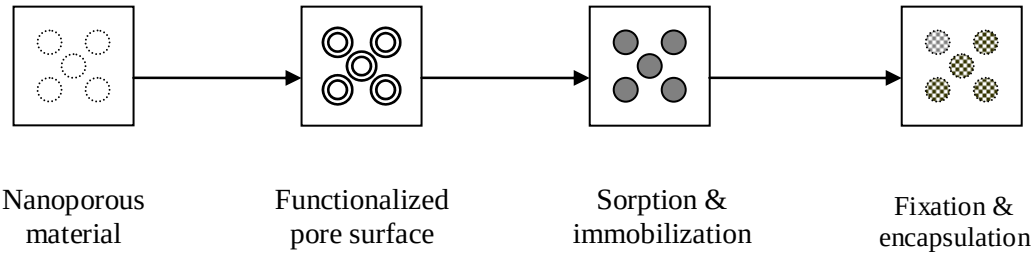

Figure 1- Formation of a nanocomposite waste form. In the final waste form, nano-scale radionuclide precipitates are embedded in a glass or ceramic matrix.

Unlike the existing waste forms, which tend to incorporate radionuclides into rigid crystal structures (Xu and Wang, 2000; Fortner et al., 2002; Ewing, 2006; Grambow, 2006), the newly developed waste forms incorporate radionuclides as nano-scale inclusions in a host matrix and thus effectively relax the constraint of crystal structure on waste loadings. Therefore, the new waste forms are able to accommodate a wide spectrum of radionuclides with high waste loadings and low leaching rates. Since the leaching rates are controlled by the dissolution rate of the host mineral, it is possible to engineer a waste form that will be thermo-dynamically stable in a repository environment, by choosing an appropriate host mineral. A good analog to this is the naturally occurring nano-scale fluid inclusions in mineral crystals, which remain intact over millions of years. It is anticipated that SNL-NCP materials can be easily integrated into the fuel reprocessing system currently proposed for advanced fuel cycles.

4. Synthesis of Nanoporous Metal Oxides

More than 300 nanoporous metal oxide materials have been synthesized, with a sol-gel route developed specifically for this project. In this route, inorganic metal salts are used as precursors, a block copolymer as a nanostructural template, and an epoxy (propylene oxide in this case) as a proton scavenger. The synthesis can be conducted under relatively simple ambient conditions from room temperature to 65 ^{o}C. A nanoporous metal oxide is obtained by drying the resultant gel at 80 ^{o}C and calcining it at a temperature at or below 600 ^{o}C in air or oxygen atmosphere. Since it uses inexpensive inorganic precursors, the synthesis route we developed can be scaled up for a large quantity of production if needed.

Use nanoporous alumina as an example. This material can be synthesized as follows: The materials used for the this synthesis include: aluminum chloride hexahydrate ($AlCl_3 \bullet 6H_2O$, e.g., from Fisher), propylene oxide (C_3H_6O, PO, e.g., from Fisher), poly(ethylene glycol)-block-poly(propylene glycol)-block-poly(ethylene glycol) (P123, e.g., from Aldrich, M_n=5800), and anhydrous alcohol (e.g., from Fisher Acros). For solution A, about 12 grams of P123 are dissolved in about 72 mL alcohol (anhydrous). For solution B, about 34 g of $AlCl_3 \bullet 6H_2O$ is dissolved in about 90 mL of a H_2O/C_2H_5OH (1:1) mixture, and then 47 g of PO is added. A typical preferred synthesis process is to mix the two prepared homogeneous solutions (A and B) for about 15 min, then set the mixture at a room temperature in the hood for about 3 days for gelation, and then dry it at about 80 degrees C in the oven for about 24 hours to turn it into a gel. The gel is then calcined at about 600 degrees C for about 4 hours at a temperature ramp of about 5 degrees C/min.

The involvement of a structural directing agent and the control of the polymerization rate of alumina hydroxides are two important factors for this synthesis. Block copolymer P123 (or other copolymer) is used as a template for nanostructures. The polymerization rate is controlled by adding a certain amount of propylene oxide (or ethylene oxide or other epoxy) to solution B. Aluminum ion, Al^{3+}, in solution has a great tendency to form positively charged polynuclear species (hydroxoaluminum complex) as follows:

$$Al^{3+} + 2H_2O \text{ --> } Al(OH)^{2+} + H_3O^{+} \ (\log K_1 = -5) \quad (1)$$

$$7Al^{3+} + 34H_2O \text{ --> } Al_7(OH)_{17}{}^{4+} + 17H_3O^{+} \ (\log K = -48.8) \quad (2)$$

$$13Al^{3+} + 68H_2O \text{ --> } Al_{13}(OH)_{34}{}^{5+} + 34H_3O^{+} \ (\log K = -97.4) \quad (3)$$

Propylene oxide in the solution acts as a proton scavenger by the nucleophilic reaction towards ring-opening. This reaction is not only irreversible but also slow, thus maintaining a uniform pH gradient in the solution for hydrolyzing aluminum salt.

The synthesis route has also been adapted to one-pot syntheses of nanoporous materials containing multiple metal components (e.g., Ag-Al, Ni-Al, or Bi-Al oxides). This one-pot process allows us to ensure the chemical and structural homogeneity of synthesized composite material. A nanoporous Ni-Al oxide material obtained using this route is shown in Figure 2. The structural homogeneity of this material is confirmed with transmission electron microscopic (TEM) observations.

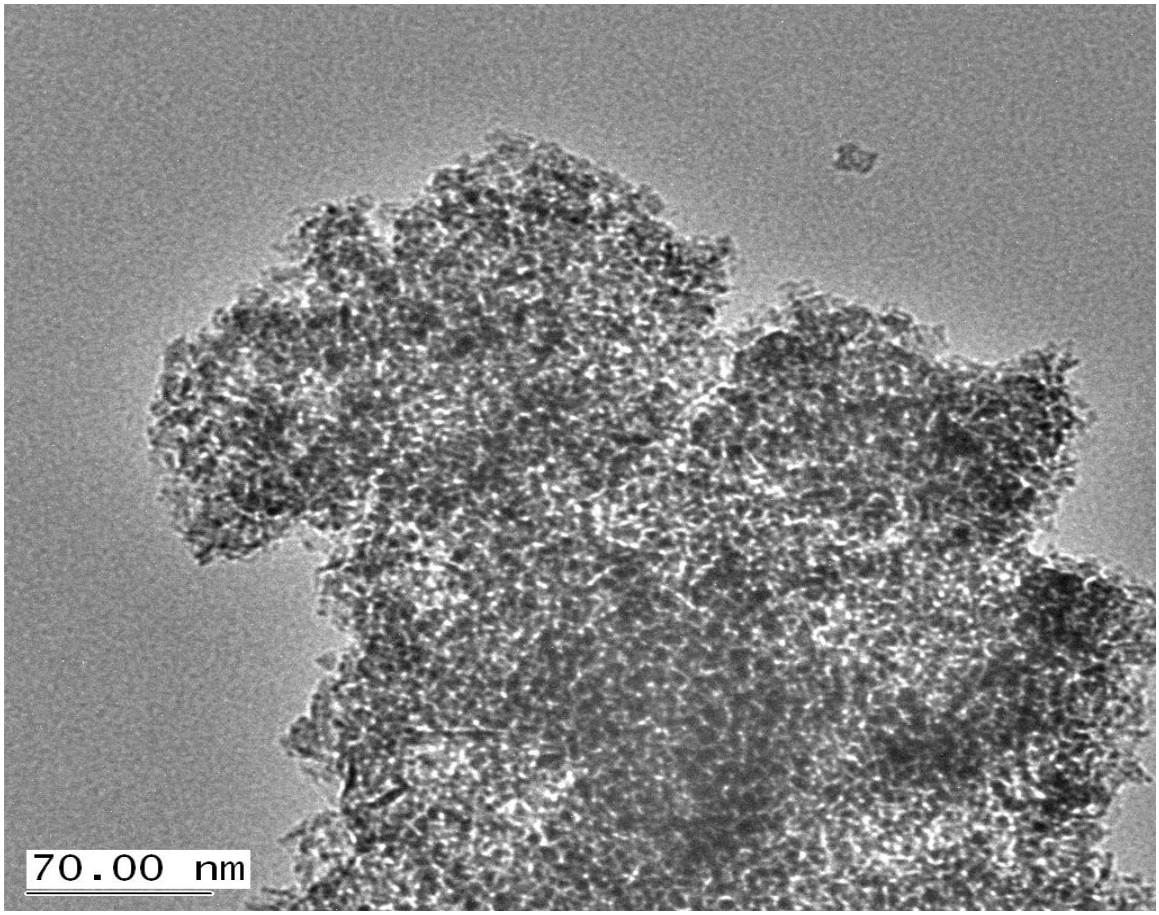

Figure 2- Transmission Electron Microscopic (TEM) image of nanoporous Ni-Al oxides, showing worm-like nanopore structures.

The synthesized materials were characterized with a powder x-ray diffractometer (XRD, Burker D8 Advance), surface area and porosity analyzer (BET TriStar 3000, Micromeritics), and transmission electron microscope (TEM, Jeol). The XRD analyses generally indicate that the synthesized materials have low crystallinity (Figure 3). The BET measurements show that these materials have pore sizes ranging from 11 to 16 nanometers and surface areas from 320 to 450 m^2/g (see Table 1, Figure 4).

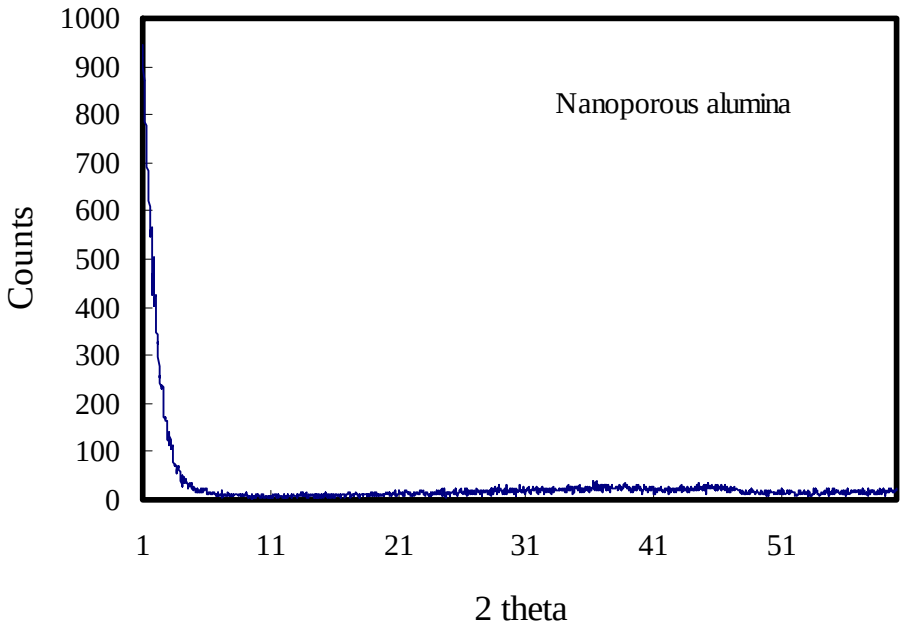

Figure 3- Powder x-ray diffraction analysis of nanoporous alumina, indicating low crystallinty of the material.

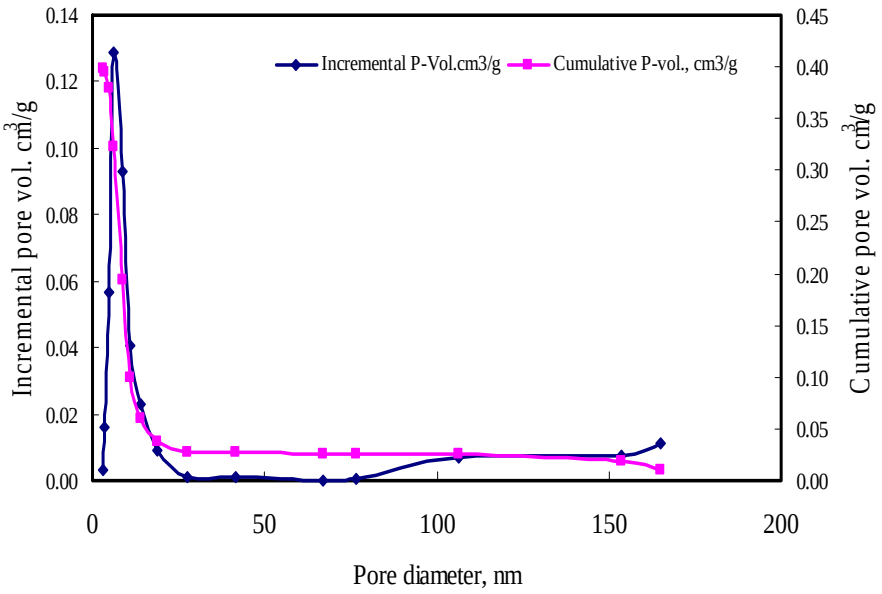

Figure 4- Pore size distribution of Ni-Al (Ni:Al = 1:1) nanoporous material determined from BET measurements.

Table 1- BET surface area, pore volume, and pore size of synthesized nanoporous alumina

		Pore volume, cm^3/g	Pore size, nm
Sample ID	Single point surface area, m^2/g	Single point (ads.)	(Ads. Average)
Nanoporous-alumina (commercial)	263.63	0.49	7.21
NC 13-A-600C/air	415.83	1.53	14.69
NC 13-A400C/O2	447.25	1.35	11.87
NC 13-B-600C/air	336.90	1.38	15.78
NC20-1 (m-Al batch 4)	319.35	1.13	13.65

5. Radionuclide Sorption on Nanoporous Metal Oxides

A set of SNL-NCP and other related materials were selected and tested for the sorption of gaseous iodine under simulated fuel reprocessing conditions. These tests provide important information regarding the selectivity of materials for iodine sorption and the potential interference of other chemical components anticipated to be present in off-gas stream of fuel reprocessing.

The tests were performed under elevated temperature (90°C) and variable relative humidity conditions, as well as with or without CO_2 and NO_2 gas added in the headspace. The general experimental setup for iodine sorption testing is shown in Figure 5. The materials tested for iodine sorption include various SNL-NCP materials (NC-77), Al-Mg layered double hydroxides (NC-88) calcined at different temperatures, mesoporous silica, activated alumina (particles), sepiolite, palygorskite, and zeolite. These materials, all inorganic, encompass diverse chemical compositions and mineral structures and thus help to mechanistically understand iodine sorption on SNL NCP materials. After each iodine sorption test, the sorbent was mixed with SiO_2 and iodine concentrations in the adsorbent were measured with an ARL QUANT'X Energy-Dispersive X-Ray Fluorescence (EDXRF) Spectrometer (Thermo Electron Corporation).

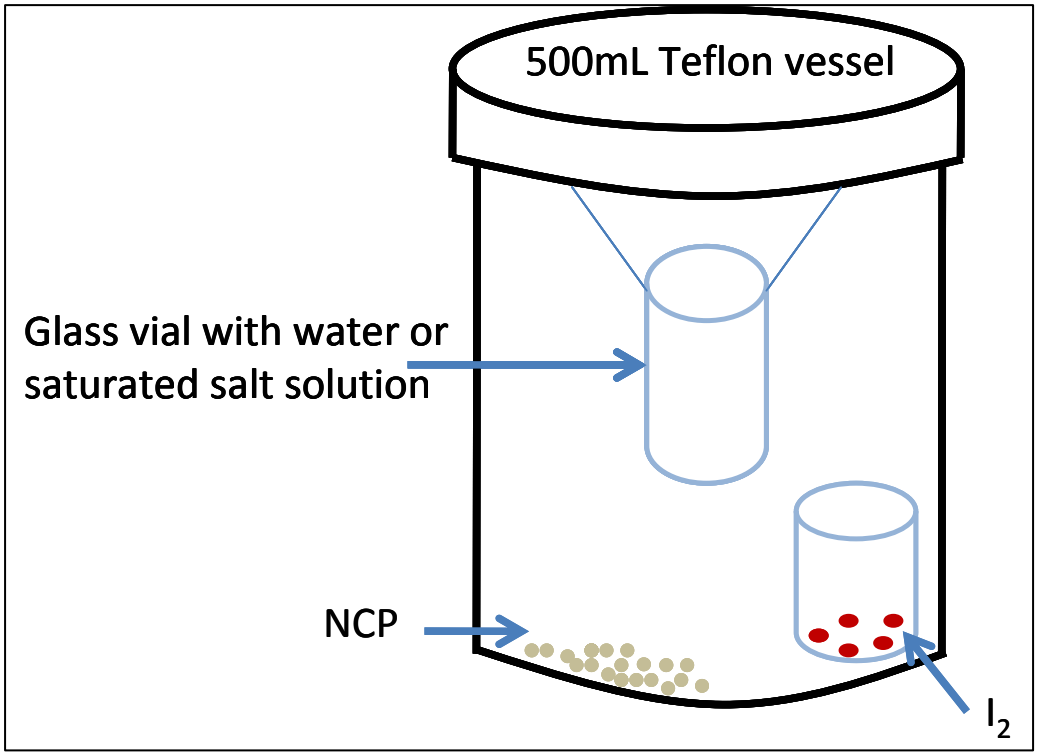

Figure 5- Experimental setup for testing iodine sorption under various relative humidity conditions. The relative humidity inside the glass vial is controlled by a saturated salt solution.

5.1 Iodine and technetium sorption

Sorption capabilities of the synthesized nanoporous metal oxides were tested using radionuclide I and Tc. Some of the results are shown in Table 2. All these materials have exhibited high sorption capabilities for I_2 and TcO_4^-. A typical iodine sorption isotherm is shown in Figure 6. The data were obtained from exhaustion experiments, in which the iodine-loaded material was heated overnight at about 90 ^oC and cooled to about room temperature in an open jar. The change in the slope of the isotherm may reflect the transition from monolayer sorption to multi-layer sorption and eventually to pore condensation as the mass ratio of iodine to adsorbent increases. The high sorption capability of Ag-Al material indicates that Ag^0 in this material tends to distribute at or close to the nanopore surfaces in the one-pot synthesis such that it is readily available for reacting with I. It was also found that I sorbed in the Ni-Al material forms a separate Ni-Al-I phase in nanopores, which may be responsible for the high I sorption capability observed. This leads the possibility of using Ni or other metals, rather than relatively expensive Ag, for immobilizing I in a final waste form.

Table 2- Sorption capability of nanoporous metal oxides for iodine and technetium

Materials	Specific surface area (m^2/g)	Pore size (nm)	Target radionuclides	Sorption capability
Alumina (Al_2O_3)	300-450	12-14	I	[I] = 2 - 4x10^3 ppm
Ag-Al oxide	200	6.5	I	[I] = 1.9-4.0x10^4 ppm
Ni-Al oxide	260	7	I, Tc*	[I]=2x10^4 ppm K_d=210 mL/g for Re
Bi-Al oxide	160	7	I, Tc*	K_d=1680 mL/g for Re

*Rhenium is used as the surrogate of Tc.

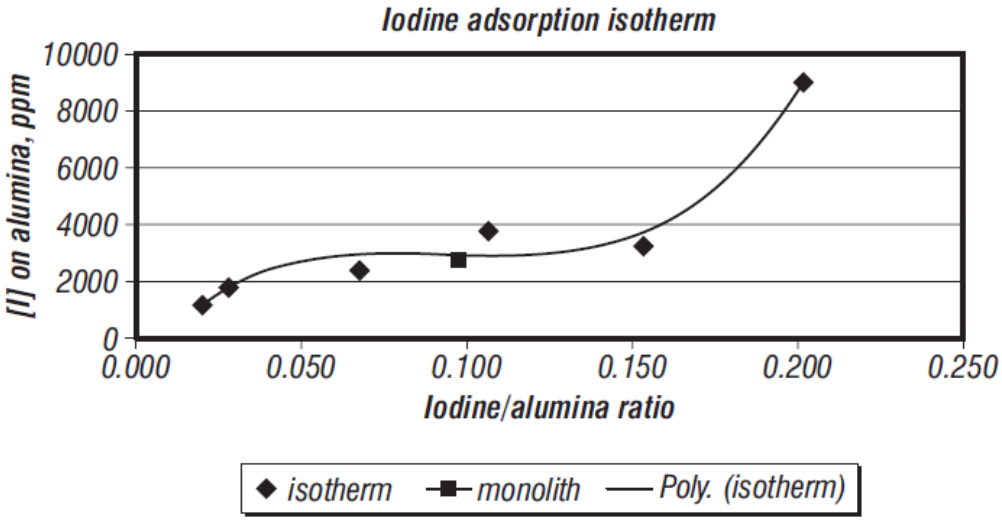

Figure 6- Isotherm of iodine adsorption on nanoporous alumina. Measurements were made after overnight desorption at 90oC following adsorption

Our work performed so far has confirmed our original finding that nanoporous Al oxide and its derivatives have high iodine sorption capabilities. To understand the mechanism, the same sorption experiment was performed on nanoporous silica, which has a larger surface area and a smaller pore sizes than the alumina materials. Interestingly, no significant I sorption was observed on the silica material, implying that the surface chemical identity of the material plays an important role in I sorption. On the other hand, we have also found that nanoporous structures can greatly enhance I sorption onto alumina (see Section 7.2). These observations indicate that the high I sorption capabilities of nanoporous alumina and its derivatives are attributed to the combined effects of surface chemistry and nanopore confinement. This points a possibility of optimizing material performance for its sorption capability and selectivity by manipulating material compositions and structures.

To understand the control of material composition on iodine sorption, a series of nanoporous metal oxides with various metal combinations and molar ratios were synthesized and tested for iodine sorption. The results are summarized in Figure 7. Al-Ni combination seems to have the highest iodine sorption capability among all the materials tested. In addition, 1:1 Al/Ni molar ratio seems to provide the better performance than other ratios.

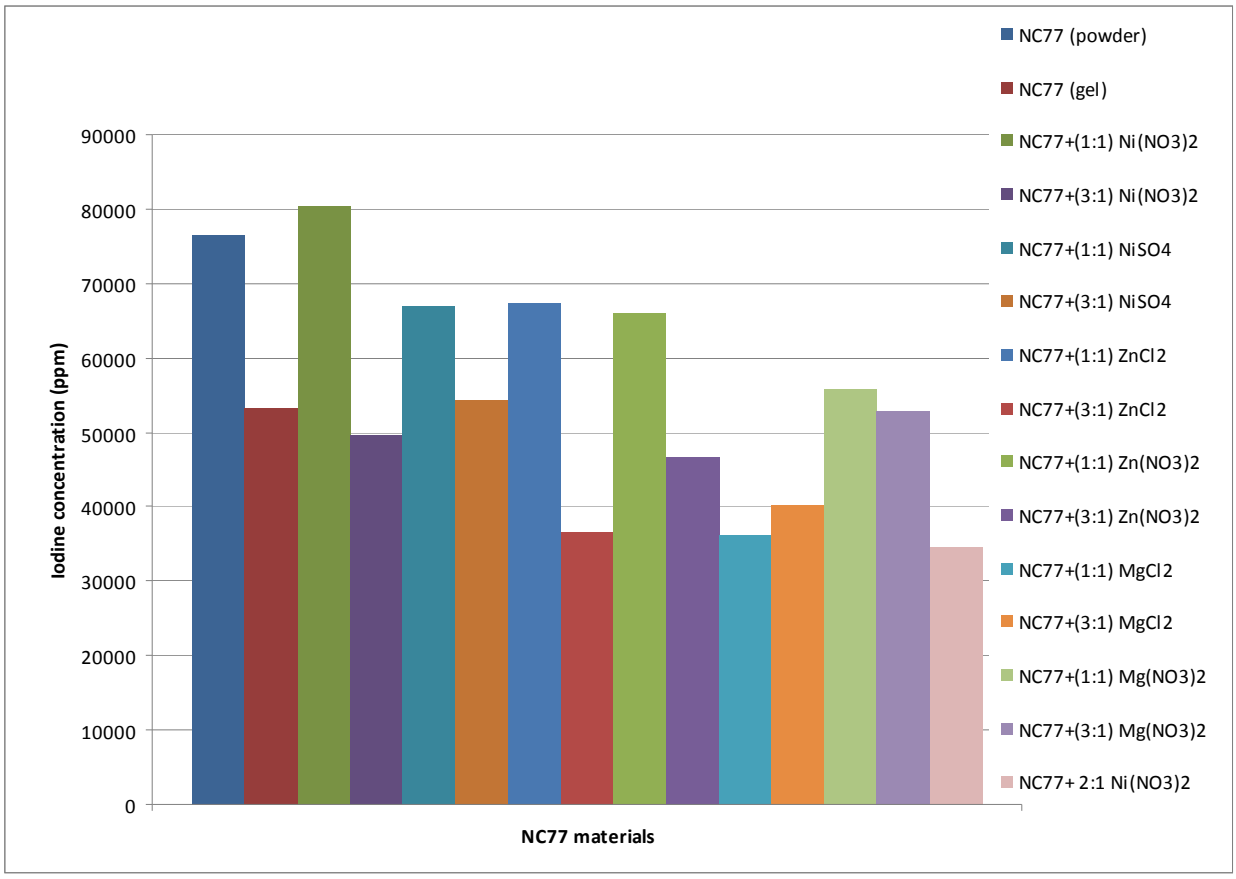

Figure 7- Iodine sorption on various nanoporous metal oxides synthesized using the one-pot sol-gel method. NC77 is pure alumina; NC77+ is a Al-M(II) oxide, where M(II) is a divalent metal. The ratios in the labels are molar ratios of M(II) to Al.

5.2 Iodine sorption under various relative humidity

The experimental setup for iodine sorption tests under a controlled relative humidity is shown in Figure 5. The relative humidity (RH) in the headspace was controlled by the presence of a saturated salt solution in the test vessel. The salt solutions used include: LiCl - RH 10.23%, $MgCl_2$ – 24.12%, KCl – 78.5%, and deionized water (DI) – 100%.

The testing results are shown in Figure 8. The following observations can be made based on the testing results:

- Nanoporous materials NC-77 and NC77-N2 outperform most of the other materials tested over the whole relative humidity range. SNL-NCP materials are relatively insensitive to water interference for iodine sorption. This unique property is important for the potential use of SNL-NCP materials as an iodine scavenger in the off-gas treatment during fuel reprocessing.

- Two layered double hydroxide materials NC88-380 and NC88-600, which can be considered as nanostructured layered materials, also exhibit high iodine sorption capabilities under high relative humidity.

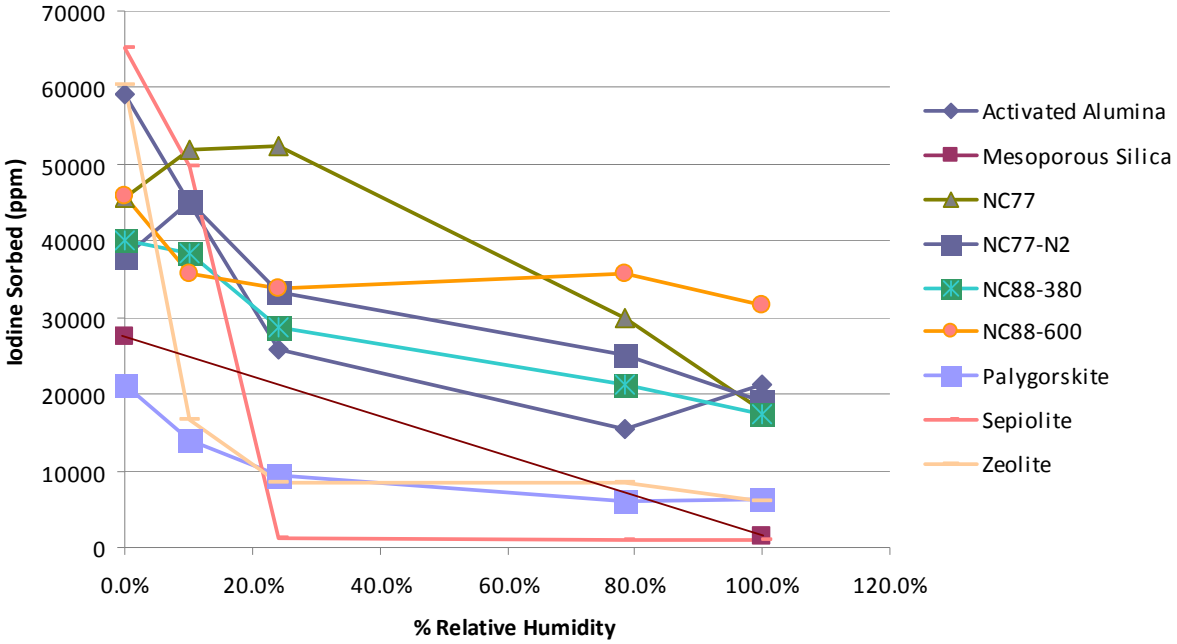

Figure 8- Iodine sorption onto SNL-NCP and other related materials under variable relative humidity

- Sepiolite and palygorskite are two naturally occurring silicate materials with similar tunnel structures and slightly different chemical compositions. The two materials, however, display distinct sorption behaviors. Particularly, sepiolite is very sensitive to water vapor, even though its sorption capability for iodine is high at zero relative humidity. This is because sepiolite generally has a high affinity for polar molecules such as H_2O.

- Mesoporous silica has a relatively lower iodine sorption capability as compared with SNL-NCP materials with a similar nanoporous structure, indicating the surface chemical identity of the material plays an important role in iodine sorption.

- Zeolite materials also show a low sorption capability for iodine. Ag-exchanged zeolite materials have been recommended for iodine capture (Jubin, 1994, Gombert, 2007). Our result indicates that the zeolite component itself does not contribute much to the iodine sorption capability of these materials, thus casting a doubt on the necessity of using zeolite as a supporting material for iodine capture.

5.3 Iodine sorption in the presence of other gaseous species

The same set of materials was also tested for iodine sorption in the presence of CO_2 and NO_2 in the headspace of the vessel. In each test, a certain quantity of solid was added to a 500 mL Teflon vessel, which was then flushed with either CO_2 or NO_2 for 15 minutes. After flushing, a glass vial containing iodine was immediately introduced into the vessel. The vessel was then sealed and placed in a 90°C oven for 6 hours.

The test results for NC77, palygorskite, and sepiolite are quite surprising. Compared to the baseline sorption tests under ambient conditions, these materials exhibit enhanced iodine sorption due to the presence of CO_2 (Figure 9). Note that these materials possess either nanopores or micropores (< nm). Thus, the test results seem to indicate a synergistic effect between CO_2 and iodine sorption in a confined pore space. The actual mechanism for this enhancement is yet to be worked out. In contrast, the test results definitely show that the presence of NO_2 results in the reduction of iodine sorption, to various extents, on all the materials tested (Figure 9).

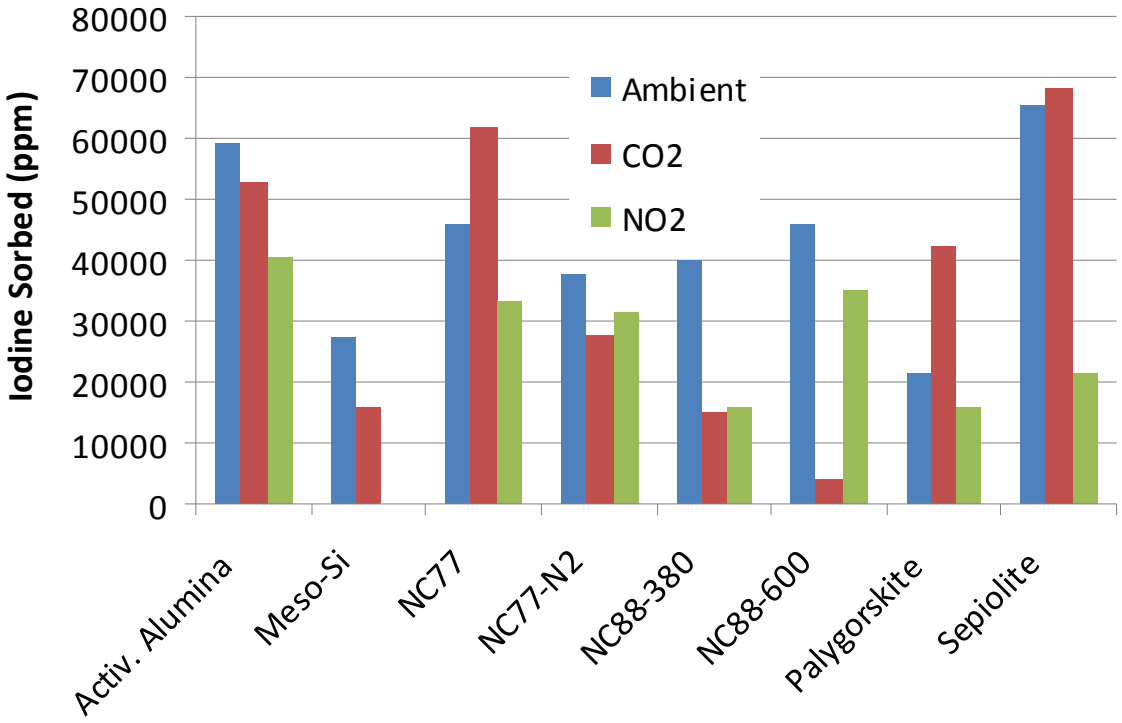

Figure 9- Iodine sorption in the presence of CO_2 or NO_2

5.4 Effect of temperature

The effect of temperature on iodine sorption is shown in Figure 10. Relatively large uncertainties may exist with these measurements, partly due to the difficulties related to iodine sublimation and condensation as the temperature varies. Nevertheless, the data seem to indicate that there is an optimal temperature range (50 – 90 ^{o}C) for iodine sorption.

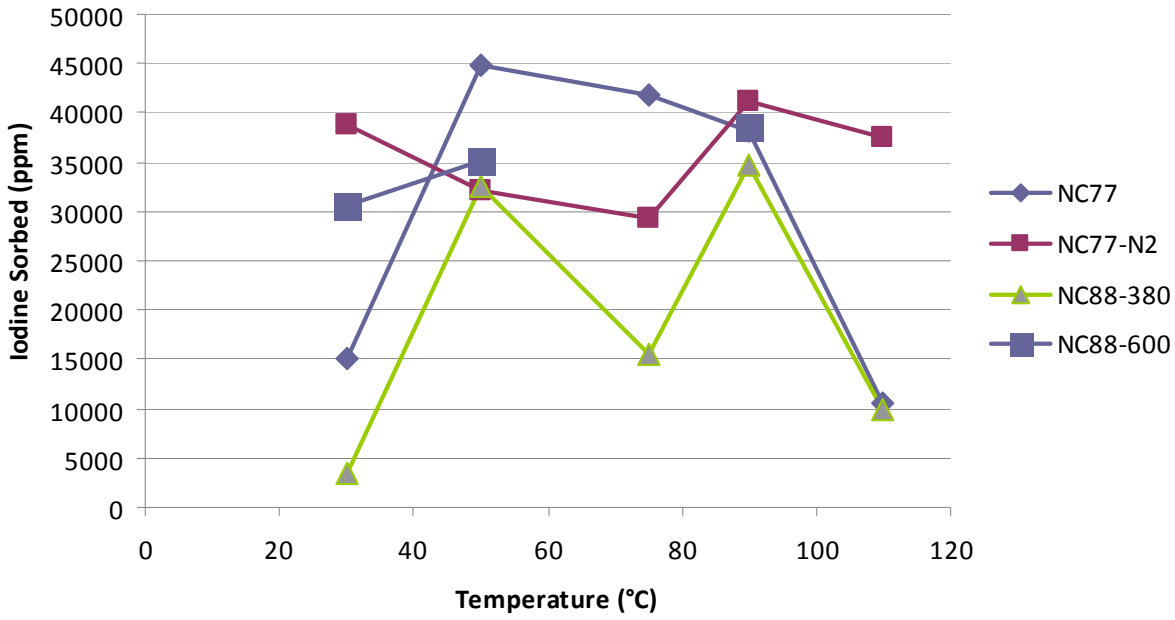

Figure 10- Effect of temperature on iodine sorption

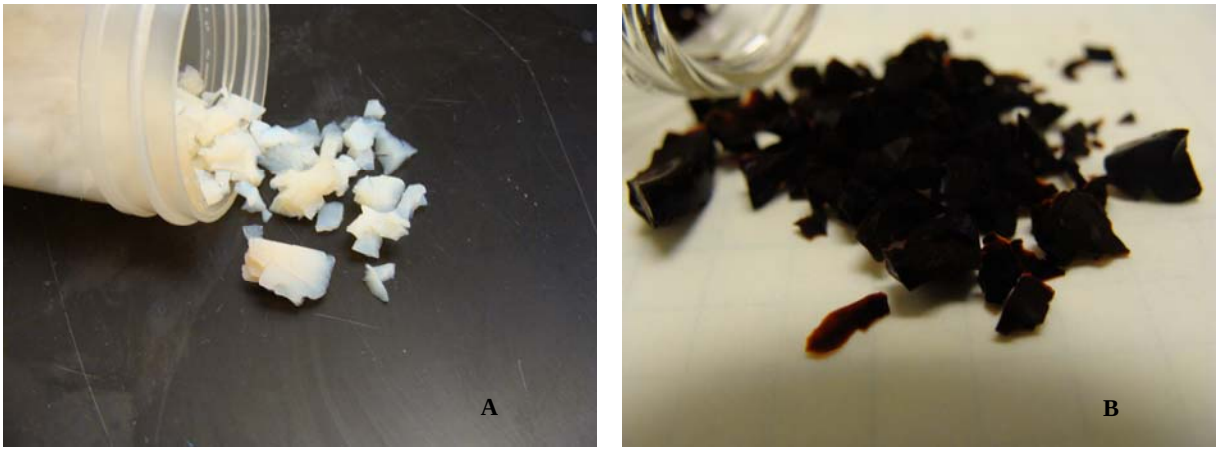

Figure 11- Formation of monolithic nanoporous SNL-NCP-A. A – before I sorption; B – after I sorption. Each individual grain has nanoporous structures. The dark brown color in B indicates that the monolithic material has a high I sorption capability. The size of monolithic grains ranges from mm to cm.

5.5 Performance of monolithic SNL-NCP materials and role of silver (Ag)

SNL-NCP materials can also be engineered into monolithic forms (Figure 11). Monolithic materials are generally preferred for engineering handling. As shown in Table 3, a monolithic form of SNL-NCP has an iodine sorption capability as high as the corresponding powder, indicating molecular diffusion in nanopores is not a limiting step for adsorption. Also, note that monolithic nanoporous alumina without silver incorporated has at least the same comparable iodine sorption capability as the nanoporous alumina with Ag included. Therefore, Ag may not be needed for I sequestration if nanoporous alumina is used as a getter material.

Table 3- Iodine sorption on nanoporous alumina and its derivatives

Material	I/(m-Al) ratio	Sample wt, g	[I] uptake, ppm	
Nanoporus alumina w/ Ag	0.114	0.2036	35674	
Monolithic Nanoporous alumina w/o Ag	0.107	0.2035	66245	
BET measurements				
Material	Surface area, m^2/g	Pore vol. cm^3/g	Pore size, nm	Micropore vol. cm^3/g
Nanoporus alumina w/ Ag	215	0.706	12.7	0.006644
Monolithic Nanoporous alumina w/o Ag	354	1.75	19.15	0.014549

6. Testing of Nanoporous Metal Oxides for Noble Gas Sorption

Batch experiments have been performed to test the feasibility of using SNL-NCP materials for noble gas adsorption. There are four different methods for adsorption measurements: (1) volumetric/manometric; (2) gravimetric; (3) carrier gas; and (4) calorimetric (Keller and Robens, 2003). In this study, the gravimetric method was adopted, and it was implemented using a vacuum microbalance in Netzsch STA 409 thermal gravimetric analyzer (TGA) with differential scanning calorimeter (DSC) and dDifferential temperature analyzer (DTA) (Figure 12).

Figure 12- Experimental setup for measurements of noble gas adsorption

In a typical measurement, the mass of a sample is first measured with a Mettler Toledo AT 261 Delta Range balance with a precision to 0.0001 g (0.1 mg). The total sample mass is usually about 100 mg. Then, the sample is placed into a small crucible and loaded in the TGA. After that, the system is purged to vacuum, followed by continuously backfilling a target noble gas to the desired pressures. Following that, the sample is analyzed with the desired adsorption noble gas by using an automated profile. The typical analytical profile is as follows: (1) heating to 90 ^{o}C; (2) maintaining at 90 ^{o}C for two hours (desorption step); (3) cooling to room temperature; and (4) maintaining at room temperature for two hours (adsorption step). The amount of adsorbed noble gas is determined by subtraction of a sample analysis from an instrumental blank. The instrumental blank is made by employing the same, but empty crucible, which is used for sample analyses. The profile for the instrumental blank and a sample analysis is the same. Analytical instruments using materials which are known to have extremely low adsorption capacities such as quartz and hydromagnesite are also run with the same profile and subtracted from the instrumental blank.

Another analytical profile is as follows: (1) heating to 140 ^{o}C; (2) maintaining at 140 ^{o}C for two hours (desorption step); (3) cooling to room temperature; and (4) maintaining at room temperature for two hours (adsorption step). This profile is used to investigate whether some structures or functional groups favorable to adsorption could be destroyed at higher temperatures.

Materials tested for noble gas adsorption include Sandia-developed nanocomposites (NC 77, NC 95, SNL-CBD series, Log#339, Log#355, S159-2-B, S185-4, S185-5, and S189-1),

activated carbon (S51HF, DARCO, and Alfar Aesar), zeolite (MP zeolite, 13X zeolite, Wacko zeolite, Spectrum zeolite, modernite-A, and modernite-N) and layered Al-silicates (silicate-P and silicate-S). As shown above, materials NC 77 and NC 95 have high sorption capabilities for iodine. Materials SNL-CBD series are nanostructured organic-inorganic composites engineered to retain high sorption capabilities of carbon-based materials but eliminate the potential fire hazard associated with these materials. Activated carbon and zeolite are included for comparison because both materials are known to adsorb noble gases. The testing results are summarized in Tables 4 through 8.

6.1 Adsorption capacities

The following observations can be made for the adsorption capacities of the tested materials:

- In the experiments with Ar at 0.9 atm (Table 4), activated carbon materials DARCO and S51HF have higher adsorption capacities than other materials, followed by activated carbon Alfar Aesar, SNL-CBD-1, SNL-CBD-2, silicate-S, NC 77, and NC 95. These samples have adsorption capacities higher than 0.30%. Mordenite, silicate-P, SNL-CBD-5B, Log#339, Log#355, S159-2-B, S185-4, S185-5, and S189-1 have adsorption capacities between 0.10% and 0.30%. The adsorption capacities for all other materials are below 0.10%. The Ar sorption on MP zeolite is very low.

- In the experiments with Kr at 0.9 atm (Table 5), DARCO, SNL-CBD series, mordenite, silicate-P, silicate-S, Wako zeolite have much higher adsorption capacities for Kr than other materials. MP zeolite, Spectrum zeolite, and calcium citrate tribasic (earlandite) exhibit relatively high selectivity for Kr over Ar.

- SNL-NCP material NC 77 has a comparable sorption capability as zeolite materials for Kr Table 5). Since SNL-NCP materials have much larger pores than zeolites, SNL-NCP materials are expected to have a much faster sorption rate than zeolite.

- Sandia-developed organic-inorganic nanocomposites (SNL-CBD series) have higher adsorption capacities than mordenites; and their adsorption capacities are comparable to those of activated carbon (Table 5).

- Naturally occurring layered silicates (silicate-P and silicate-S) have adsorption capacities comparable to those of mordenites (Table 5).

- In the experiments with Ar with 2 hours desorption at 140 ^{o}C followed by 2 hours adsorption at room temperature (Table 6), the surface property of NC 77 apparently changed, resulting in a relatively low sorption capability. The detailed mechanism for this change is currently under investigation. However, the surface functional groups favorable for Ar adsorption in S51HF and DARCO remain unchanged.

- The preliminary results at pressure lower than 0.9 atm are presented in Table 7. The amount of noble gas adsorbed was reduced accordingly at a low gas pressure.

Table 4- Adsorption Experiments with Ar at room temperature and 0.9 atm (685 torr) pressure*

Adsorbents	Weight percentage of noble gas adsorbed (wt.%)
MP zeolite	0.00
Zeolite 13X	0.08
NC 77	0.33
NC 95 (unground)	0.23
NC 95 (ground)	0.31
S51HF	0.68
Hydromagnesite	0.02
DARCO	0.72
Activated Carbon (Alfar Aesar)	0.50
SNL-CBD-1	0.42±0.06
SNL-CBD-2	0.37±0.01
SNL-CBD-5B	0.24
Log#339	0.175±0.005 (average of un-ground and ground samples)
Log#355 (unground)	0.14
S159-2-B (unground)	0.20
Silicate-P	0.26
Silicate-S	0.36
Mordenite-N	0.27
Mordenite-A	0.12
Spectrum zeolite	0.03
Wako zeolite	0.07
Spectrum $Al(OH)_3$ (Spectrum Chemical MFG Corp)	0
S185-4	0.19
S185-5	0.13
S187	0.01
S188	0.05
S189-1	0.10
S189-2	0.02
Brucite (Fisher Scientific)	0.00
Nesquehonite (Synthetic)	0.00
Calcium citrate tribasic (earlandite) (ACROS ORGANICS)	0.00

*Samples are first subjected to 2 hours desorption at 90 ^{o}C, and then 2 hours adsorption at room temperature in the vacuum microbalance.

Table 5- Adsorption Experiments with Kr at room temperature and 0.9 atm (685 torr) pressure*

Adsorbents	Weight percentage of noble gas adsorbed (wt.%)
MP zeolite	0.36±0.08
Zeolite 13X	0.64
NC 77	0.24
Hydromagnesite (Synthetic)	0.05
DARCO	3.60
SNL-CBD-1	3.01
SNL-CBD-2	2.51
Silicate-S	0.71
SNL-CBD-3[A]	1.93
SNL-CBD-3B[A]	1.97
SNL-CBD-3C	2.56
SNL-CBD-4	1.63
SNL-CBD-5	2.69
SNL-CBD-6	2.06
Mordenite-N	1.74
Mordenite-A	1.31
Silicate-P	1.03
Wako zeolite	0.99
Spectrum zeolite (Spectrum Chemical MFG Corp)	0.53
Calcium citrate tribasic (earlandite) (ACROS ORGANICS)	0.16
S159-2-B	0.30
S185-4	0.30
S185-5	0.42
S187	0.29
S188	0.39
S189-1	0.32
S189-2	0

* Samples are first subjected to 2 hours desorption at 90 ^{o}C, and then 2 hours adsorption at room temperature in the vacuum microbalance.

[A] Sample spill outside of the crucible was observed; therefore this value represents a minimum value.

Table 6- Adsorption Experiments with Ar at room temperature and 0.9 atm (685 torr) pressure*

Adsorbents	Weight percentage of noble gas adsorbed (wt.%)
NC 77	0.03
S51HF	0.58
DARCO	0.48
SNL-CBD-2	0.46[A]

*Samples are first subjected to 2 hours desorption at 140 ^{o}C, and then 2 hours adsorption at room temperature in the vacuum microbalance.
[A] Sample spill outside of the crucible was observed; therefore true value should be higher than this.

Table 7- Adsorption Experiments with Ar at room temperature and 0.2 atm (170 torr) pressure*

Adsorbents	Weight percentage of noble gas adsorbed (wt.%)
MP Zeolite	0.0[A]
SNL-CBD-2	0.16[A]

*Samples are first subjected to 2 hours desorption at 90 ^{o}C, and then 2 hours adsorption at room temperature in the vacuum microbalance.
[A] Sample spill outside of the crucible was observed; therefore this value represents a minimum value.

6.2 Adsorption kinetics

Adsorption kinetics is important to noble gas separation and thus of great practical significance in capturing radioactive noble gases from spent fuel reprocessing. Unfortunately, there is little published data that is directly relevant to the systems of our interest. For instance, numerous studies have been done on the kinetics of krypton adsorption on a number of metal surfaces at temperatures below the triple point of argon (–157 ^{o}C) by using various techniques (e.g., Carlsson and Madix, 2001).

Based on the measurements of the amounts of noble gases adsorbed on an adsorbent material as a function of time, we have calculated the rate constants of noble gas adsorption on the various materials we have tested. The calculation is illustrated in Figures 13 and 14. Figure 13 shows the amount of Kr adsorbed on SNL-CBD-5 measured as a function of time until the attainment of adsorption saturation at a partial pressure of 0.9 atm at room temperature. For simplicity, the initial linear part of the adsorption curve was used to constrain the adsorption rate constant (Figure 14).

Constrained adsorption rate constants are presented in Table 8. It is interesting to note that MP zeolite, Spectrum zeolite, and calcium citrate tribasic (earlandite) seem to be able to

adsorb selectively Kr over Ar, as the ratios of adsorption rate constants of k_{Kr} to k_{Ar} are higher than 10 (Table 8). Also note that the adsorption capacities of MP zeolite and calcium citrate tribasic for Ar are zero (Table 4), and thus the adsorption rate constants of these materials for Ar are equivalently infinitely small. For this reason, we assign the adsorption rate constants for Ar as one order of magnitude smaller than their corresponding adsorption rate constants for Kr.

Mordenites and Wako zeolite have similar k_{Kr}/k_{Ar}. Silicate-p and silicate-S have similar adsorption rate constants for both Ar and Kr, and therefore their k_{Kr}/k_{Ar} are close to 1. SNL-CBD series samples have higher adsorption rate constants for Kr than all zeolites, silicate-P and silicate-S, and their k_{Kr}/k_{Ar} ranges from 2.88 to 8.14. Adsorption rate constants of DARCO activated carbon for both Ar and Kr are higher than the other samples investigated. NC 77 seems to have a higher adsorption rate constant for Ar than for Kr. This is opposite to the trend of all other test materials. We are in the process of expanding the study of this material.

Mordenite, especially Ag-mordenite, has been considered as a candidate for adsorption of radioactive noble gases (e.g., Ianovski et al., 2002; Munakata et al., 2003, 2006, 2008). It seems that materials developed at Sandia National Laboratories can outperform modernite-A and mordenite-N in terms of adsorption capacities and adsorption kinetics, in addition to their inexpensive nature. Naturally occurring silicate-P and silicate-S can also compete with modernite-A and mordenite-N in terms of adsorption capacity for Kr, even though their adsorption rate constants are lower than those of modernite-A and mordenite-N.

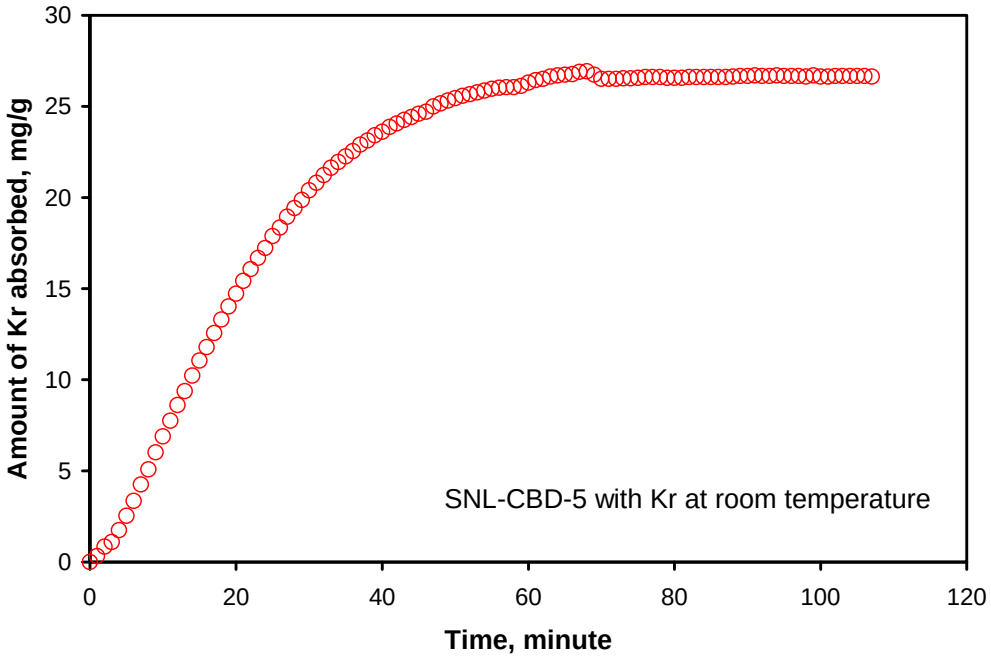

Figure 13- Amounts of Kr absorbed on SNL-CBD-5 as a function of time until attainment of saturation equilibrium.

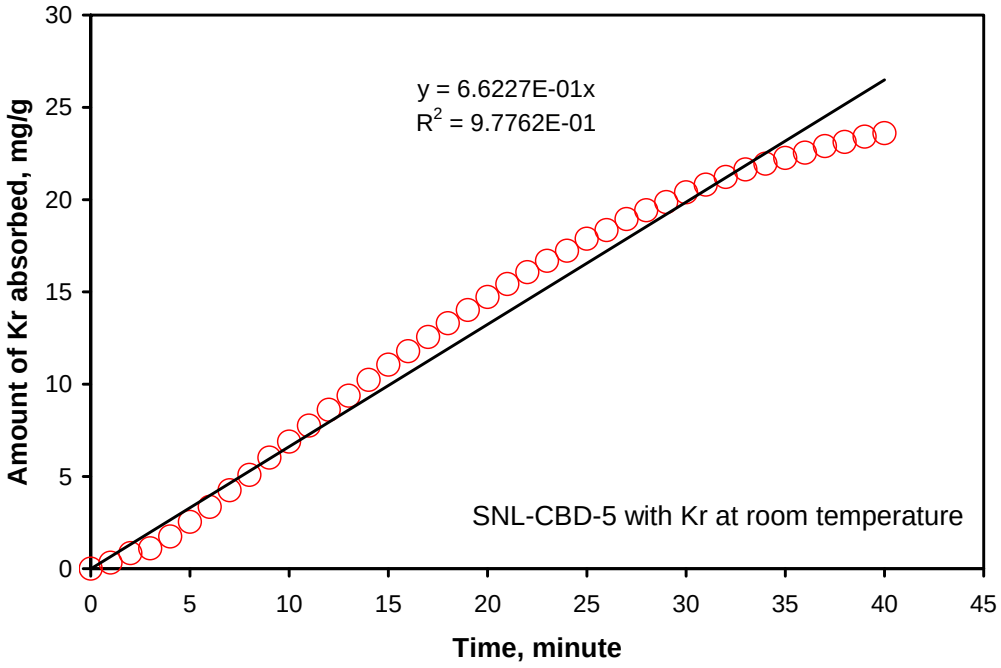

Figure 14- Constraining an adsorption rate constant from the initial part of adsorption curve.

Table 8- Adsorption rate constants determined from experiments at 680 torrs and 25 °C

Material	Noble gas adsorbed	Adsorption rate constant (k_{Ar} or k_{Kr}), mg/g min^{-1}
Mordenite-A	Argon	4.10×10^{-2}
Mordenite-A	Krypton	2.53×10^{-1}
k_{Kr}/k_{Ar}		6.17
Mordenite-N	Argon	8.84×10^{-2}
Mordenite-N	Krypton	5.00×10^{-1}
k_{Kr}/k_{Ar}		5.66
MP Zeolite	Argon	$< 5.22\times10^{-3}$
MP Zeolite	Krypton	5.22×10^{-2}
k_{Kr}/k_{Ar}		> 10
Zeolite 13X	Argon	5.35×10^{-2}
Zeolite 13X	Krypton	1.74×10^{-1}
k_{Kr}/k_{Ar}		3.25
Spectrum Zeolite	Argon	5.52×10^{-3}
Spectrum Zeolite	Krypton	7.96×10^{-2}

k_{Kr}/k_{Ar}		14.4
Wako Zeolite	Argon	2.12×10^{-2}
Wako Zeolite	Krypton	1.60×10^{-1}
k_{Kr}/k_{Ar}		7.55
Silicate-S	Argon	1.94×10^{-1}
Silicate-S	Krypton	2.41×10^{-1}
k_{Kr}/k_{Ar}		1.24
Silicate-P	Argon	1.44×10^{-1}
Silicate-P	Krypton	2.20×10^{-1}
k_{Kr}/k_{Ar}		1.53
SNL-CBD-1	Argon	2.59×10^{-1}
SNL-CBD-1	Krypton	7.46×10^{-1}
k_{Kr}/k_{Ar}		2.88
SNL-CBD-2	Argon	1.52×10^{-1}
SNL-CBD-2	Krypton	6.67×10^{-1}
k_{Kr}/k_{Ar}		4.39
SNL-CBD-3C	Krypton	6.41×10^{-1}
SNL-CBD-4	Krypton	3.86×10^{-1}
SNL-CBD-5B	Argon	8.13×10^{-2}
SNL-CBD-5	Krypton	6.62×10^{-1}
k_{Kr}/k_{Ar}		8.14
SNL-CBD-6	Krypton	4.94×10^{-1}
S185-5(ground)	Argon	5.90×10^{-2}
S185-5(ground)	Krypton	7.87×10^{-2}
k_{Kr}/k_{Ar}		1.33
S187	Argon	8.44×10^{-3}
S187	Krypton	4.91×10^{-2}
k_{Kr}/k_{Ar}		5.82
S189-1	Argon	1.58×10^{-2}
S189-1	Krypton	7.75×10^{-2}
k_{Kr}/k_{Ar}		4.91
NC77	Argon	1.36×10^{-1}
NC77	Krypton	4.86×10^{-2}

k_{Kr}/k_{Ar}		0.357
DARCO activated carbon	Argon	3.66×10^{-1}
DARCO activated carbon	Krypton	9.95×10^{-1}
k_{Kr}/k_{Ar}		2.72
Alfar Aesar activated carbon	Argon	1.59×10^{-1}
S-51HF activated carbon	Argon	2.97×10^{-1}
Calcium Citrate Tribasic	Argon	$< 2.89\times10^{-3}$
Calcium Citrate Tribasic	Krypton	2.89×10^{-2}
k_{Kr}/k_{Ar}		> 10

7. Conversion of Nanoporous Metal Oxides Into Waste Forms

7.1 Radionuclide fixation

A suite of techniques have been developed for the fixation of radionuclide in metal oxide nanopores. The key to this fixation is to chemically convert a target radionuclide into a less volatile or soluble form. Iodine can be fixed in two ways: (1) introducing Ag to a getter material to convert I_2 into AgI upon sorption and (2) adding a chemical base (e.g., Na_4SiO_4) to an I_2-loaded material to covert I_2 to iodide or iodate ions. X-ray photoelectron spectra (XPS) show that 66% of I_2 is converted to I^- upon iodine sorption onto Ag-alumina nanoporous material (Figure 15). Similarly, Fourier Transformation Infrared spectroscopic (FTIR) analysis indicates that adding Na_4SiO_4 during I fixation forces the sorbed iodine gas in the nanopores to completely convert to I^- and IO_3^-, thus significantly reducing iodine volatility. Our work indicates that the second approach is preferred for I fixation. We have also found that the same method may apply to Tc fixation. Preliminary data indicate that addition of Na_4SiO_4 or NaOH helps convert TcO_4^- into insoluble TcO_2. The detailed mechanism for this conversion still needs to be clarified.

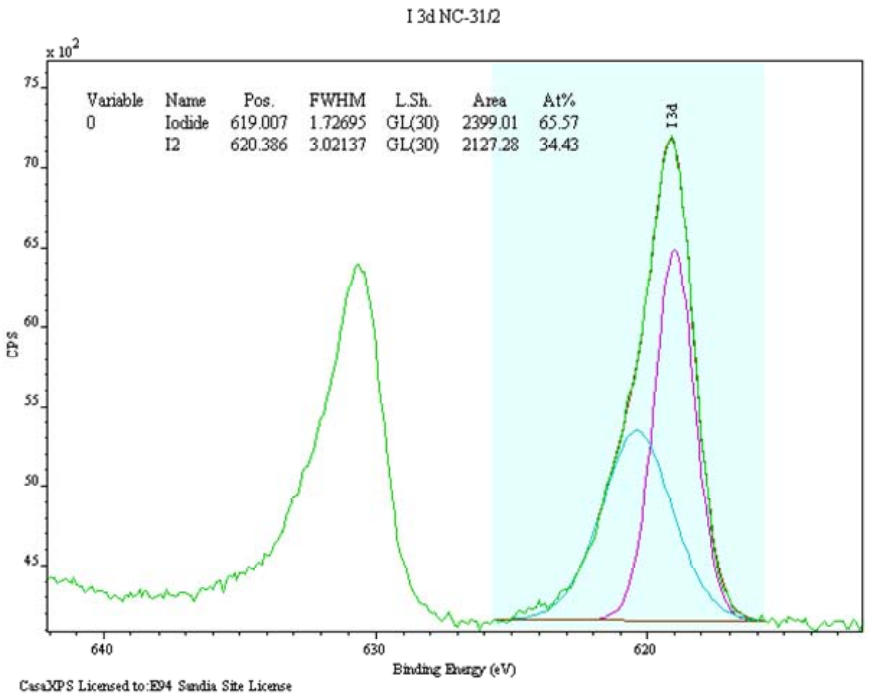

Figure 15- X-ray photoelectron spectra (XPS) showing 66% of I_2 converted to I^- upon iodine sorption onto Ag-alumina nanoporous material.

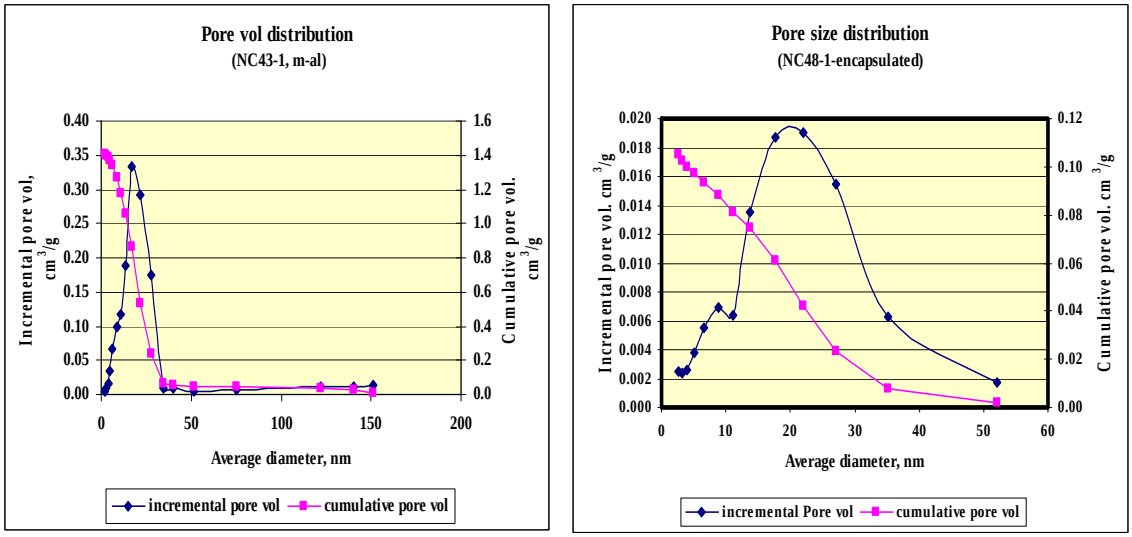

Figure 16- Effective sealing of nanopores with Na-silicate solution. Left – pore volume distribution before sealing; Right - pore volume distribution after sealing.

7.2 Radionuclide encapsulation

Radionuclides loaded onto a getter material are encapsulated by pore sealing and vitrification. We have found that mixing a radionuclide-loaded getter material with a certain amount of Na-silicate solution can effectively (>90%) seal the nanopores in the material (Figure 16), thus enhancing radionuclide retention during subsequent vitirification of the material. As a matter fact, no significant I loss was observed during vitrification if nanoporous alumina is used as an iodine getter.

A pore-sealed material is then mixed with a glass-forming frit and vitrified to form a glass-ceramic waste form. We have tested six commercially available frits for their ability to isolate radionuclides. We have found that Fero frit "510" – a lithium borosilicate material – produces the best result. Figure 15 shows some of glass-ceramic waste forms produced using the proposed nano-immobilization and nano-encapsulation technique. In these waste forms, radionuclide nanoparticles are embedded in either amorphous or crystalline matrix (Figure 17).

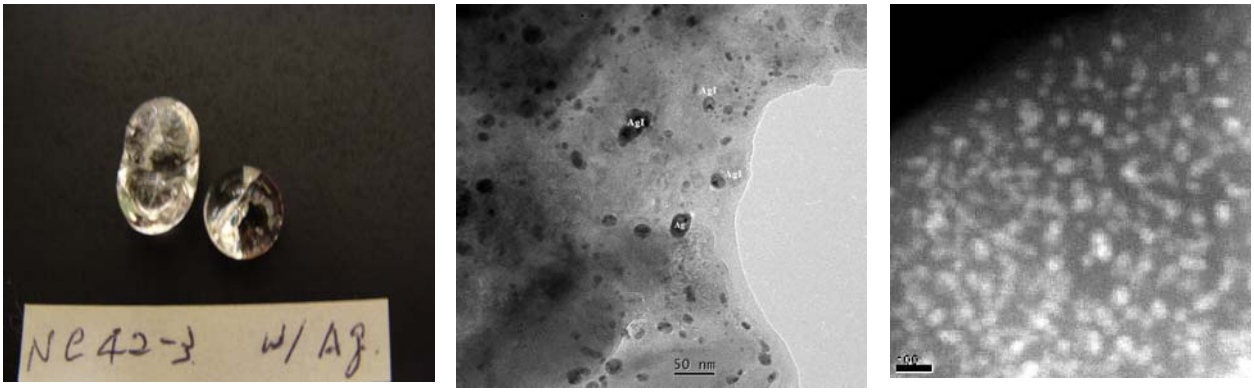

Figure 17- Glass-ceramic waste forms produced using the proposed technique. Nanoparticles embedded: left – AgI-embedded glass –ceramic waste form; middle – TEM image of AgI-waste form; right – image of Bi-Tc waste form. Re is used as analog to Tc.

Furthermore, as shown in Table 9, with the radionuclide fixation and encapsulation developed for this project, the loss of iodine during the conversion of an iodine-loaded nanoporous material into a waste form is minimal even at 1100 ^{o}C. It is clear that nanoporous structures not only enhance I sorption but also help to retain I during the fixation and encapsulation (Table 10).

Table 9- Iodine loadings on glass-ceramic materials

Glass sample	[I] in the ceramic-glass, ppm	[I], normalized to mass (g) of mesoporous alumina, ppm	vitrification temperature, ^{o}C	Iodine loss % during vitrification*
NC48-1+ "510"	429	7064	1100	32
NC48-2 + "510"	915	15067	1100	0
NC48-1 +"XF140-2"	698	11494	1100	0
NC48-2 +"XF140-2"	1069	17603	1100	0
NC52-2 + "3225"	617	9872	1100	5
NC52-2 + "CS749"	570	9120	1100	12
NC67-7	748	11968	1200	0
NC67-6	243	3880	1100	63
iso-750	855	13680	750	0
ios-800	649	10384	800	0
iso-850	659	10544	850	0
iso-900	706	11296	900	0
* Non-zero numbers are due to the heterogeneity of samples.				

Table 10- Effects of nanoporous structures on I sorption and retention by alumina materials

Material	I sorption (ppm)	% of I lost during fixation	% of I lost during vitrification
Alumina particles	98	Not tested	Not tested
Activated alumina	8700	45	65
Nanoporous alumina	25000	0	0

7.3 Leaching tests of glass-ceramic waste forms

The obtained waste forms were subject to short-term leaching tests. The results are summarized in Table 11. Three observations can be made from the table: First, nanoporous alumina (m-Al-I) fixed with potassium silicate provides the best performance in the leaching tests. Second, a material with no Ag incorporated performs better than the same materials fixed with silver. Therefore, silver may not be necessary for iodine immobilization in a glass-ceramic waste form. Third, there exists an optimal temperature for vitrification. This temperature is about 850-950 ^{o}C, which is lower than that used for glass formation (generally > 1100 ^{o}C). It is likely that the formation of nano-scale crystalline mineral phases at the optimal temperature enhances waste form durability. This has been confirmed by high temperature X-ray diffraction (HTXRD) analyses (Figure 18).

Table 11- Summary of leaching tests

Material	pH-end	Iodine loss, %	vitrification T, ^{o}C	[SiO_2], ppm	composition
First leaching test (LA)					
LA-1	9.29	14.5	1100	not analyzed	m-Al-I+Na4SiO4+"510"
LA-2	9.50	27.4	1100	not analyzed	m-Al-Ag-I+Na4SiO4+"510"
LA-3	8.18	38.5	1100	not analyzed	m-Al-I+Na4SiO4+"XF140-2"
LA-4	8.22	33.3	1100	not analyzed	m-Al-Ag-I+Na4SiO4+"XF140-2"
m-Al-I /silver composite					
LB-1	8.40	37.4	1100	44	3225+NC52-2(vit),
LB-2	8.39	19.6	1100	44	CS749+NC52-2(vit)
LB-3	10.31	40.6	1100	717	m-Al-I + Na4SiO4
LB-4	10.66	29.6	1100	664	m-Al-I + Na4SiO4
LB-5	8.02	40.6	1100		m-Al-I+Na4SiO4 +SiO2+B2O3
LB-6	8.28	15.9	1200	27	m-Al-I+Na4SiO4 +SiO2
m-Al-I samples w/o silver					
LC-1	10.30	5.8	750		750 C. m-Al-I+Na4SiO4+"510" frit
LC2	10.12			1666	750 C. m-Al-I+Na4SiO4+"510" frit
LC-3	9.86	7.8	800	1034	800C. m-Al-I+Na4SiO4+"510" frit
LC-4	9.89			1013	800C. m-Al-I+Na4SiO4+"510" frit
LC-5	9.49	20.9	850	278	850C. m-Al-I+Na4SiO4+"510" frit
LC-6	9.52			419	850C. m-Al-I+Na4SiO4+"510" frit
LC-7	9.17	29.4	900	250	900C.m-Al-I+Na4SiO4+"510" frit
LC-8	9.18			213	900C. m-Al-I+Na4SiO4+"510" frit
m-Al-I samples fixed with potassium silicate					
LD-1	9.96	0.0	750	1444	750 C. m-Al-I+Na4SiO4+"510" frit
LD-2	10.02	0.0		2145	750 C. m-Al-I+Na4SiO4+"510" frit
LD-3	9.74	0.0	800	987	800C. m-Al-I+Na4SiO4+"510" frit
LD-4	9.52	0.0		497	800C. m-Al-I+Na4SiO4+"510" frit
LD-5	9.20	0.0	850	206	850C. m-Al-I+Na4SiO4+"510" frit
LD-6	9.15	0.0		174	850C. m-Al-I+Na4SiO4+"510" frit
LD-7	8.68	13.5	900	279	900C.m-Al-I+Na4SiO4+"510" frit
LD-8	8.94	7.6		279	900C. m-Al-I+Na4SiO4+"510" frit

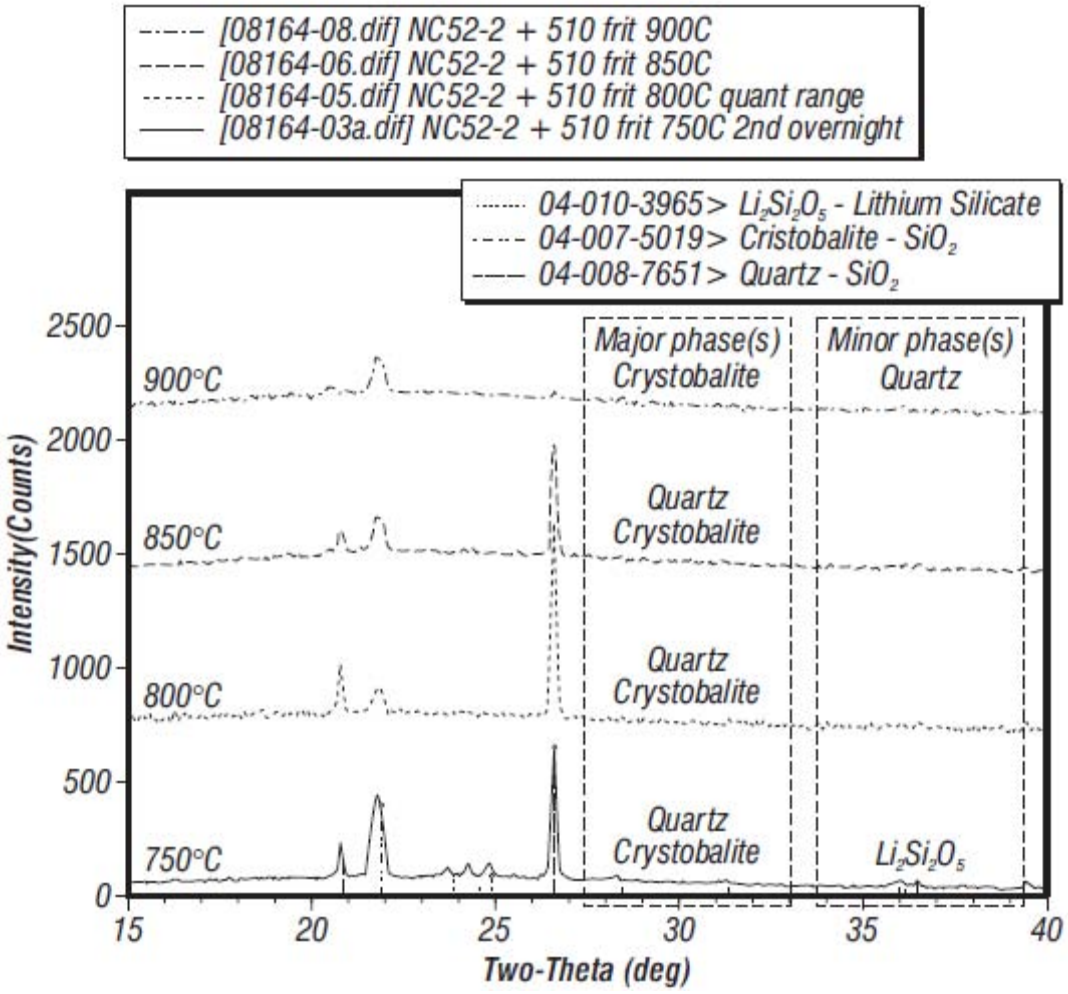

Figure 18- XRD patterns of glass-ceramic waste forms showing the crystallinity change with increasing vitrification temperatures. Quartz, crystoballite and lithium silicate occur in the 750 oC sample; these phases disappear at 900oC as the amorphous phase becomes more dominant.

The leaching rate of the waste form depends on the stability of both radionuclide-bearing nanocrytallites and their surrounding matrix. HTXRD analyses indicate that at a relatively low sintering temperature, e.g., between 750-800 ^{o}C, several crystalline phases appear (Figure 18). The leaching test result indicates that glass-ceramic waste forms vitrified at 750 ^{o}C seem to have the lowest iodine loss during leaching. This may be due to the high content of crystalline quartz (possibly as the embedding matrix) as well as the presence of crystalline lithium silicate. In the case of the glass ceramic sample containing Ag, nanocrystals of AgI are observed to be embedded in crystalline quartz. At a higher vitrification temperature, iodine anions are expected to distribute more uniformly in the resulting waste form, probably "dissolved" in the glass matrix, thus transitioning from nano-scale radionuclide encapsulation to traditional mineral structural incorporation and therefore resulting in less resistant waste forms.

8. Sorption Modeling Using Grand Canonical Monte Carlo (GCMC) Method

Adsorption isotherms were simulated using the sorption module of the Materials Studio software suite (Allen and Tildesley, 1987; Frenkel and Smith, 2002). This software suite allows for simulation of sorption isotherms under a wide variety of conditions (temperature and pressure), and has the capability of handling multiple components simultaneously (e.g. I_2 and H_2O). The parameters for a typical isotherm simulation at 363 K use the Metropolis algorithm (Metropolis et al., 1953), with $1.0x10^5$ equilibration steps, and $5x10^5$ production steps. Electrostatic summations were treated according to the Ewald method (0.001 kcal/mol accuracy) while van der Waals summations were treated with an atom based method (cubic spline cutoff of 12.5Å). The equilibration and production values are lower than many of those reported in literature, however, the very long equilibration and production cycles serve only to improve overall data statistics and have little impact on overall magnitude of the sorption isotherm.

Sorption studies have included γ–alumina (Al_2O_3), and quartz (SiO_2), with I_2, I_2 + H_2O, Kr, and Xe. The isotherms which included simultaneously both I_2 and H_2O were for direct comparison against relative humidity experimental data. Parameters for γ-Al_2O_3 are Al: σ=2.898 Å, ε=0.4916 kcal/mol; O: σ=3.627 Å, ε=0.0784 kcal/mol; while the parameters for silica: Si: σ =4.295 Å, ε=0.3000 kcal/mol; O: σ=3.511 Å, ε=0.1554 kcal/mol. Since we are using GCMC methods, the sorbate and sorbent models are static, bonding terms need not be included in the force field description.

Table 12- Lennard-Jones parameter of Ar, Kr and Xe

Species	σ (Å)	ε (kcal/mol)	q (e)
I in I_2	2.376	35.56	±0.366
Ar	3.353	0.285	-
Kr	3.571	0.400	-
Xe	3.892	0.562	-

Because of the large atomic radii of iodine and its ability to become polarized we have opted to use force-field parameters that mimic this molecular phenomenon. Lennard-Jones 6-12 parameters were used for I_2 (σ = 2.376 Å; ε = 35.56 kcal/mol) (Kornweitz and Levine, 1998); however, the individual iodine atoms of I_2 were artificially charged ($\delta^{\pm}$ = ±0.366 e) (Pasternak et al., 1977) such that molecular neutrality was maintained but a dipole is established (Figure 12). The result is a sorption analyte which accounts for the molecular polarization of I_2 when it interacts with another atom or surface. Lennard-Jones 6-12 parameters of Ar, Kr, and Xe were taken from a literature source (Goharshadi and Abbaspour, 2006) and are listed in Table 12 and shown in Figure 19.

Comparison of 363K I_2 isotherms between γ–alumina and silica indicate a more significant uptake for the alumina case (Figure 20). This is consistent with experimental observations that mesoporous silica has a low sorption capability for iodine (see Section 5.1). In addition to the maximum uptake capacity, the shape of the isotherm also indicates that the energetics is slightly more favorable in the alumina case. When we compare I_2 uptake versus relative humidity, we can clearly see that increasing the relative humidity reduces the capacity of

each material to adsorb molecular I_2 by roughly 50%. This suggests that the I_2 and H_2O are competing for the same surface adsorption sites and that there are no synergistic effects to consider, which is consistent with our experimental observations summarized in Section 5.1.

Sorption of the noble gases Kr and Xe show distinctly different behaviors. The most striking feature of these isotherms is that Xe, the larger of the two sorption analytes, shows higher uptake than the smaller Kr (Figure 21). The second feature which is readily apparent is that the uptake of alumina is significantly higher than that of silica (Figure 21). Initially differences in surface charge might be considered as a reasonable explanation. However, since the analytes themselves are not charged, surface charge should have little effect on the uptake capacity and therefore electrostatic considerations are minimal. Since electrostatic attraction is negligible the much weaker van der Waals or London dispersion forces must be considered as the source for the enhanced uptake capacity. This confirms our original postulate that molecular polarization plays important role in Kr and Xe sorption. This mechanistic understanding of noble gas adsorption will help us to improve the performance of SNL-NCP materials.

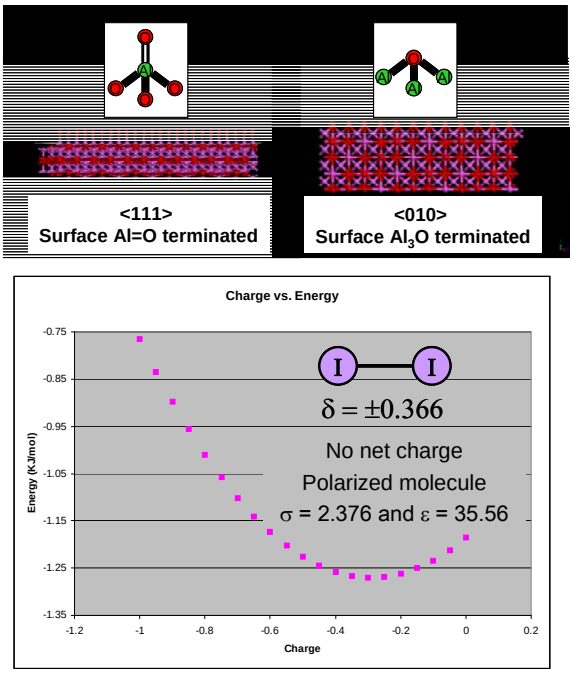

Figure 19- Model system for iodine sorption on γ-alumina

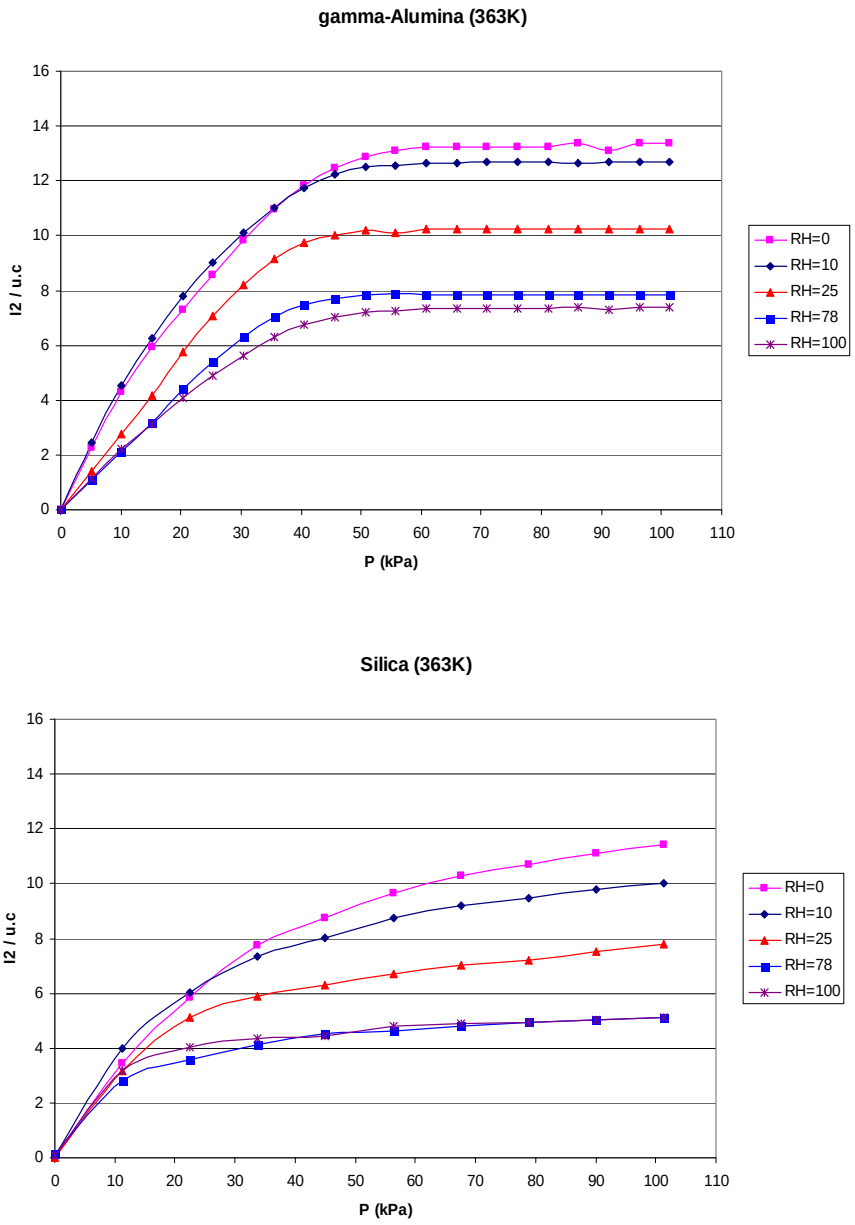

Figure 20- Molecular dynamic calculations for iodine sorption on alumina and silica surfaces at various relative humidity

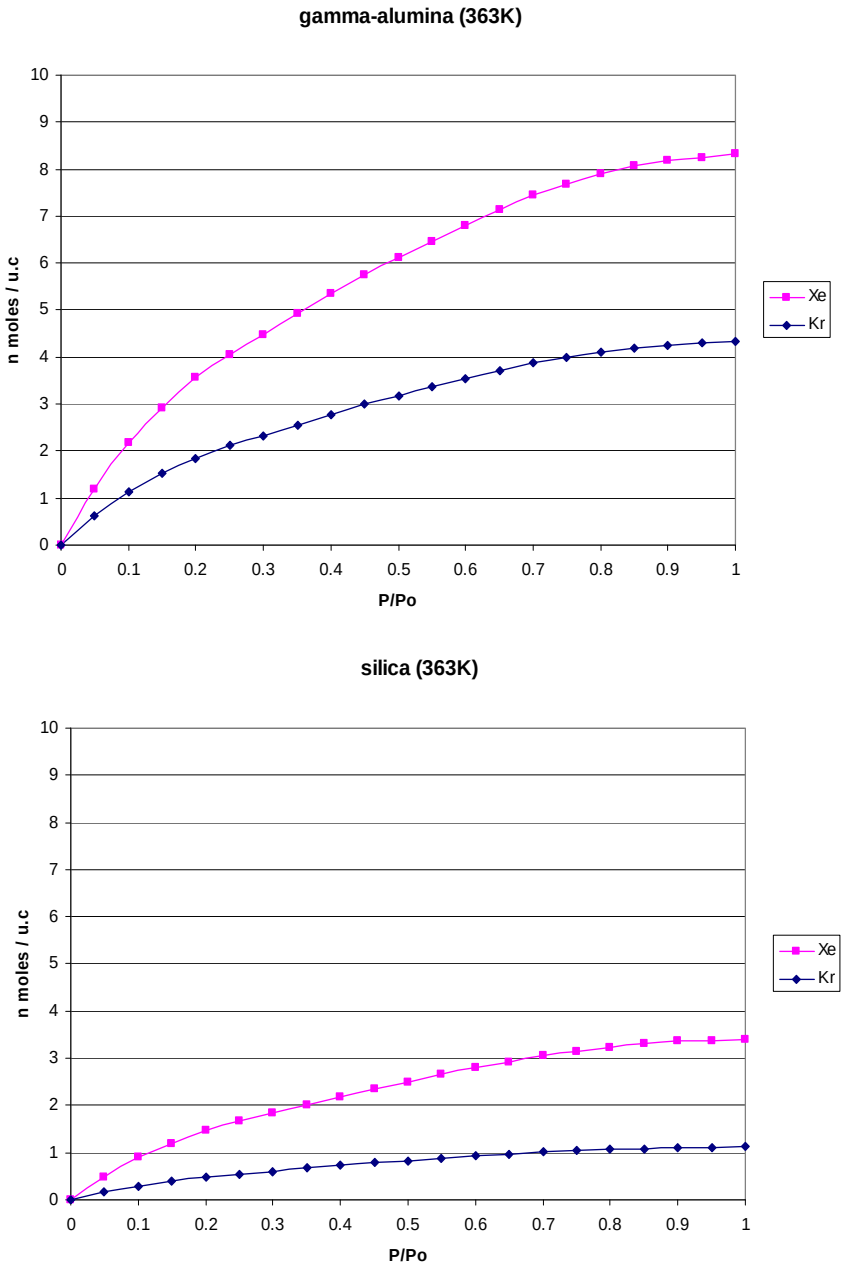

Figure 21- Molecular dynamic calculations for Kr and Xe sorption on alumina and silica surfaces

The surfaces of these two materials can be terminated structurally in several ways and this could account for the isotherm differences. The first, is termination through by a single oxygen atom bonded to a single metal (Si or Al) atom (M=O) which produces a surface with a significant regular nanostructures. The second possibility is termination by a single oxygen atom bound to three metal (Si or Al) atoms (M_3O) that produces a very uniform surface with little variation in the local nanostructure. In gamma-alumina the predominant surface termination motif is Al=O and not Al_3O and our model reflects this preference. Whereas in silica, the predominant termination motif is considered Si_3O rather than Si=O and our model also reflects this termination preference. This variation in local surface structure could potentially account for the differences we see in the isotherms; however, further simulations (specifically of the Si=O terminated silica) are necessary to prove this hypothesis.

To investigate the effect of space confinement on gaseous radionuclide adsorption, A GCMC simulation was performed for a nanopore represented by two parallelγ-alumina (Al_2O_3) <111> surfaces. The coordinate perpendicular to the planar walls was changed from 1.5 to 4 nm to simulate different pore sizes. The simulation result for I_2 sorption is s shown in Figure 22. Over the pore size range studied, the pore size from 2.5 to 3.0 nm seems to have optimal sorption performance. This result needs to be confirmed by experiments.

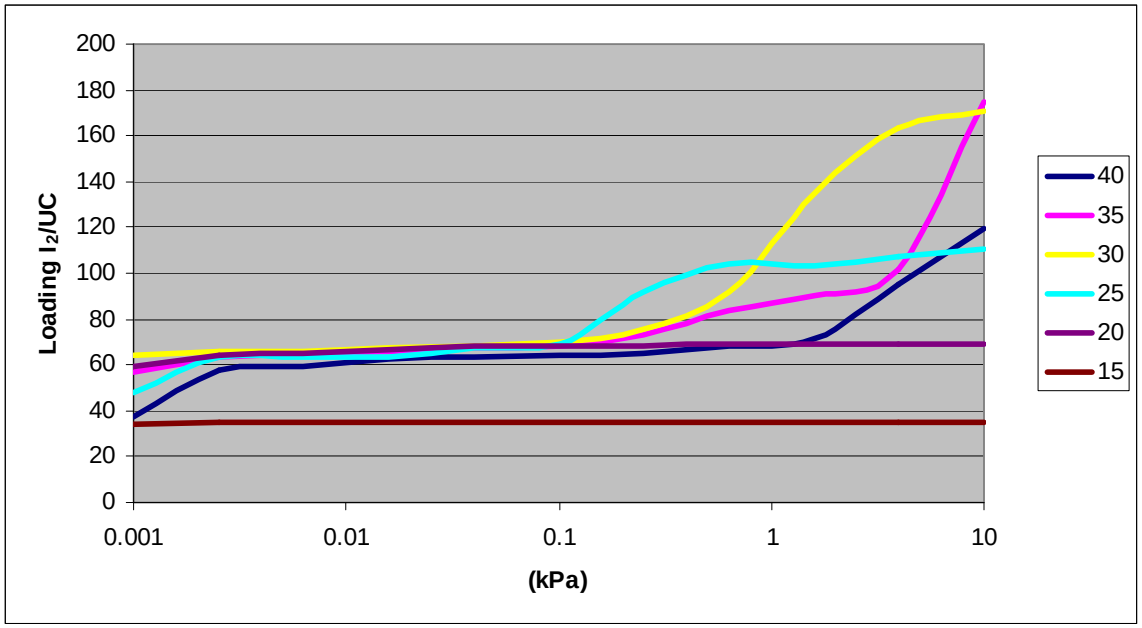

Figure 22- GCMC adsorption isotherms for iodine sorption onto alumina nanopore surfaces as a function of pore size. Numbers in the labels are pore sizes in Å.

A GCMC simulation was also performed to investigate the possibility of improving material sorption performance through surface modifications. In the study shown in Figure 23, 60% of oxygen atoms on alumina surface were replaced with F atoms. The simulation result for iodine sorption onto the fluorinated surface is shown in Figure 24. The fluorinated surface appears to have enhanced the attraction of the I_2 molecules to the surface. Based on this result, a technique to graft fluorine functional groups onto nanoporous alumina surfaces is currently under development.

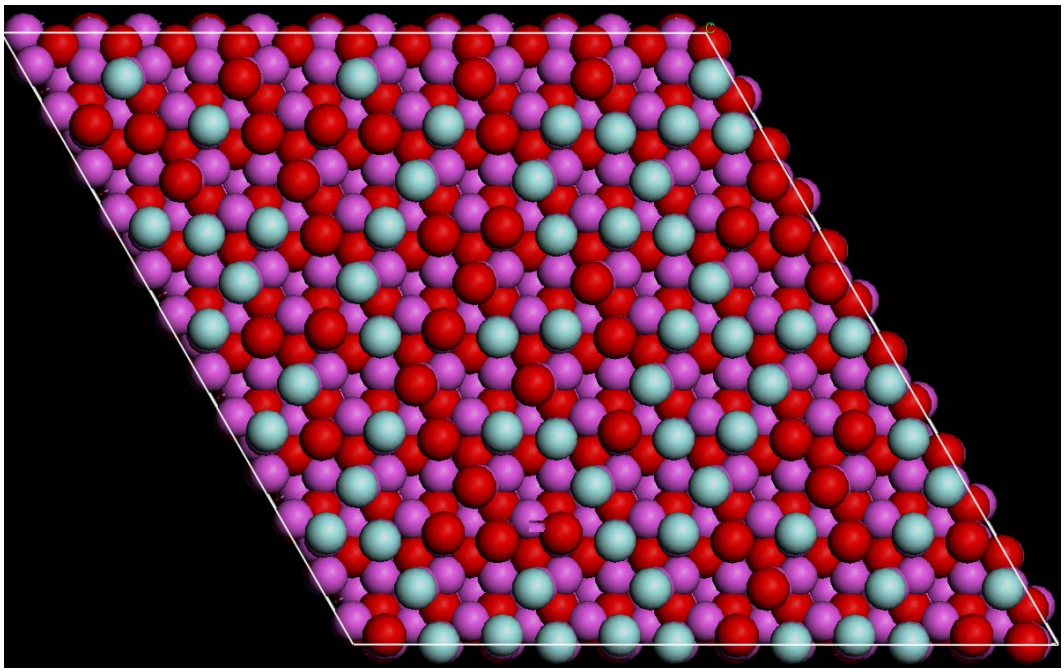

Figure 23- Plane view of 60% fluorinated alumina surface. Turquoise balls are F, Red = O and Magenta = Al.

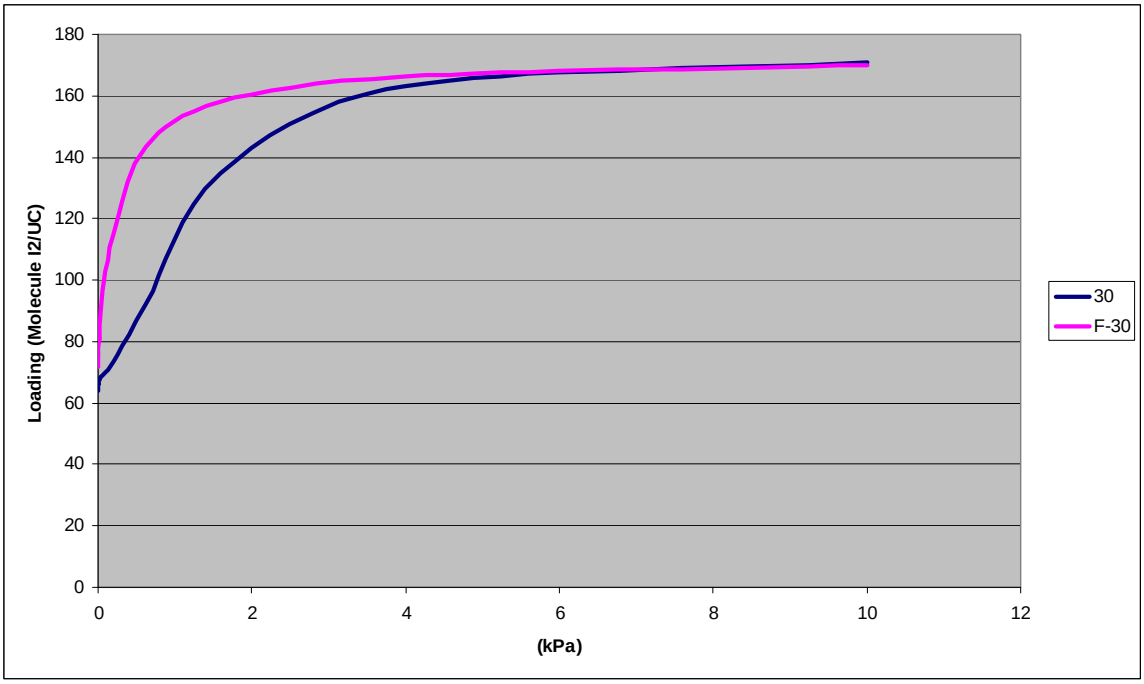

Figure 24- GCMC simulation result for iodine adsorption onto fluorinated alumina surface.

9. Conclusions

Under the support of Sandia National Laboratories (SNL) Laboratory-Directed Research & Development) (LDRD), we have developed a suite of inorganic nanocomposite materials (SNL-NCP) that can effectively entrap various radionuclides, especially for ^{129}I and ^{99}Tc. In particular, these materials have high sorption capabilities for iodine gas. After the sorption of radionuclides, these materials can be directly converted into nanostructured waste forms. This new generation of waste forms incorporates radionuclides as nano-scale inclusions in a host matrix and thus effectively relaxes the constraint of crystal structure on waste loadings. Therefore, the new waste forms have an unprecedented flexibility to accommodate a wide range of radionuclides with high waste loadings and low leaching rates.

Specifically, we have developed a general route for synthesizing nanoporous metal oxides from inexpensive inorganic precursors. More than 300 materials have been synthesized and characterized with x-ray diffraction (XRD), BET, and transmission electron microscope (TEM). The synthesized materials have been tested for their sorption capabilities for radionuclide I and Re (as an analog to Tc). The results have confirmed our original finding that nanoporous Al oxide and its derivatives have high I sorption capabilities due to the combined effects of surface chemistry and nanopore confinement. We have developed a suite of techniques for the fixation of radionuclides in metal oxide nanopores. The key to this fixation is to

chemically convert a target radionuclide into a less volatile or soluble form. We have developed a technique to convert a radionuclide-loaded nanoporous material into a durable glass-ceramic waste form through calcination. We have shown that mixing a radionuclide-loaded getter material with a Na-silicate solution can effectively seal the nanopores in the material, thus enhancing radionuclide retention during waste form formation. Our leaching tests have demonstrated the existence of an optimal vitrification temperature for the enhancement of waste form durability. Our work also indicates that silver may not be needed for I immobilization and encapsulation.

In addition, through an extensive set of iodine and noble gas sorption tests, as well as molecular modeling calculations, we have found:

- SNL-NCP materials have been demonstrated to have significant advantages over other materials for iodine sorption under high relative humidity conditions. Among the materials tested, SNL-NCP materials are the least sensitive to water interference for iodine sorption.

- Experimental data indicate a possible synergistic effect between iodine and carbon dioxide on their adsorption onto SNL-NCP materials. The presence of carbon dioxide may actually enhance iodine sorption.

- The test results also show that the presence of NO_2 results in the reduction of iodine sorption, to various extents, on all the materials tested.

- Zeolite materials show a low sorption capability for iodine, indicating that that zeolite component itself does not contribute much to the iodine sorption capability of Ag-exchanged zeolite materials and thus casting doubt on the necessity of using zeolite as a supporting material for iodine capture.

- The gravimetric noble gas sorption measurements have demonstrated the feasibility of using Sandia nanocomposite materials for Kr and Xe sorption.

- Based on the sorption experiments, a new set of SNL-NCP materials has been developed. The new materials are nanostructured organic-inorganic composites that have very high Kr sorption capabilities, comparable to that for activated carbon, but eliminate the potential fire hazard associated with activated carbon.

- The rate constants for noble gas adsorption onto a large set of adsorbent materials have been constrained, thus providing important information for designing an adsorption-based Kr and Xe capture system.

- Molecular dynamic modeling results have helped to clarify the control of surface structure and surface chemistry on iodine, krypton, and xenon sorption onto SNL-NCP materials and thus have provided the guide for future improvements to the materials.

10. References

Allen M. P. and Tildesley D. J. 1987. *Computer Simulation of Liquids*. Clarendon Press, Oxford.

Bodansky D. 2006. "Reprocessing spent nuclear fuel," *Physics Today.* December 2006, pp. 80-81.

Carlsson A.F., and Madix R. J. 2001. "Intrinsic and extrinsic precursors to adsorption: Coverage and temperature dependence of Kr adsorption on Pt(111)," *Journal of Chemical Physics.* Vol. 114, pp. 5304-5312.

Ewing R. C. 2006. "The nuclear fuel cycle: A role for mineralogy and geochemistry," *Elements*. Vol. 2, pp. 331-334.

Fortner J. A., Kropf A. J., Finch R. J., Bakel A. J., Hash M. C., and Chamberlain D. B. 2002. "Crystal chemistry of uranium (V) and plutonium (IV) in a titanate ceramic for disposition of surplus fissile material," *J. Nuclear Mater.* Vol. 304, pp. 56-62.

Frenkel D. and Smit B. 2002. *Understanding Molecular Simulation: From Algorithms to Applications, 2nd Edition.* Academic Press, San Diego.

Goharshadi E. K. and Abbaspour M. 2006. "Molecular dynamics simulation of argon, krypton, and xenon using two-body and three-body intermolecular potentials," *J. Chem. Theory Comput.* Vol. 4, pp. 920-926.

Gombert D. 2007. *Appendixes for Global Nuclear Energy Partnership Integrated Waste Management Strategy Waste Treatment Baseline Study*. Idaho National Laboratory, GENP-WAST-WAST-AI-RT-2007-000324.

Grambow B. 2006. "Nuclear waste glasses - How durable?" *Elements*, Vol. 2, pp. 357-364.

Hiejima Y., Kanakubo M., Takebayashi Y., Aizawa Y., Kurata Y., and Ikushima Y. 2006. "Phase behavior of Xe confined in porous vycor glass probed by Xe-129 NMR chemical shift," *J. Phys. Soc. Japan*. Vol. 75, pp. 024603-1-024603-4.

Ianovski D., Munakata K., Kanjo S., Yokoyama Y., Koga A., Yamatsuki S., Tanaka K., Fukumatsu T., Nishikawa M., and Igarashi Y. 2002. "Adsorption of noble gases on H-mordenite," *J. Nuclear Sci. Tech.* Vol. 39, pp. 1213-1218.

Jubin R. T. 1994. *The Mass Transfer Dynamics of Gaseous Methyl-Iodide Adsorption by Silver-Exchanged Mordenite*. Oak Ridge National Laboratory, ORNL-6853.

Kato H., Kato O., and Tanabe H. 2002. *Review of Immobilization of Techniques of Radioactive Iodine for Geological Disposal. JAERI-Conf* 2002-004.

Keller J.U., and Robens E. 2003. "A note on sorption measuring instruments," *Jounral of Thermal Analysis and Calorimetry*. Vol. 71, pp. 37-45.

Kornweitz H. and Levine R. D. 1998. "Formation of molecular iodine in high-energy four-center CH3I+CH3I collisions," *Chem. Phys. Lett.* Vol. 294, pp. 153-161.

Metropolis N., Rosenbluth A. W., Rosenbluth M. N., Teller A. H. and Teller E. 1953. "Equation of state calculations by fast computing machines," *J. Chem. Phys.* Vol. 21, 1087-1092.

Munakata K., Kanjo S., Yamatsuki S., Koga A., and Ianovski D. 2003. "Adsorption of noble gases on silver-mordenite," *J. Nuclear Sci. Tech.* Vol. 40, pp. 695-697.

Munakata K., Okabe H., Ianovski D., Kanjo S., and Igarashi Y. 2006. "Screening test for adsorbent for Kr at liquid argon temperature under nitrogen atmosphere," *Journal of Nuclear Science and Technology*. Vol. 43, 103-106.

Munakata K., Shinozaki T., Okabe H. 2008. "Adsorption of krypton on adsorbents at cryogenic temperatures," *Journal of Power and Energy Systems*. Vol. 2, p. 171-177.

NEA OECD. 2006. *Advanced Nuclear Fuel Cycles and Radioactive Waste Management*. NEA No. 5990.

Pasternak A., Anderson A. and Leech J. W. 1977. "Bond charge model for lattice-dynamics of iodine," *J. Phys. C: Solid State Phys.* Vol. 10, pp. 3261-3271.

Peters M. and Ewing R. C. 2007. "A science-based approach to understanding waste form durability in open and closed nuclear fuel cycles," *J. Nuclear Materials*. Vol. 362, pp. 395-401.

Rovnyi S. I., Pyatin N. P., and Istomin I. A. 2002. "Catching of I-129 during processing of spent nuclear fuel from power plants," *Atomic Energy*. Vol. 92, pp. 534-535.

Stephenson D.J., Fairchild C.I., Buchan R.M., and Dakins M.E. 1999. "A fiber characterization of the natural zeolite, mordenite: A potential inhalation health hazard," *Aerosol Science and Technology*. Vol. 30, pp. 467-476.

Terkikh V. V., Seidl M., and Knözinger H. 1999. "Xe-129 NMR study of xenon adsorbed on $V_2O_5/TiO_2/SiO_2$ catalysts," *Colloids and Surfaces A: Physicochemical and Engineering Aspects*. Vol. 158, pp. 249-254.

Wang Y., Bryan C., Gao H., Pohl P., Brinker C. J., Yu K., Xu H., Yang Y., Braterman P. S., and Xu Z. 2006. *Potential Applications of Nanostructured Materials in Nuclear Waste Management*. Sandia National Laboratories, Albuquerque, NM. SAND2003-3313.

Wang Y. and Gao H. 2006. "Compositional and structural control on anion sorption capability of layered double hydroxides (LDHs)," *J. Colloid Interface Sci.* Vol. 301, pp. 19-26.

Wang, Y., Gao H., Yeredla R, Xu H, and Abrecht M. 2006. "Control of surface functional groups on pertechnetate sorption on activated carbon," *J. Colloid Interface Sci.*, 305, 209-217.

Webster C. E., Cottone A. III, and Drago R. 1999. "Multiple equilibrium analysis description of adsorption on Na-mordenite and H-mordenite," *J. Am. Chem. Soc.* Vol. 121, pp. 12127-12139.

Xu H. and Wang Y. 2000. "Crystallization sequence and microstructure evolution of Synroc samples crystallized from CaZrTi2O7 melts," *J. Nuclear Mater.* Vol. 279, pp. 100-106.

Distribution

4 Lawrence Livermore National Laboratory
Attn: N. Dunipace (1)
P.O. Box 808, MS L-795
Livermore, CA 94551-0808

1	MS0370	Randall M. Summers	Org. 1433
1	MS0701	Marianne Walck	Org. 6700
1	MS0736	John E. Kelly	Org. 6770
1	MS0736	Dana A. Powers	Org. 6770
1	MS0736	Susan Y. Pickering	Org. 6760
1	MS0747	Ken B. Sorenson	Org. 6774
1	MS0754	Patrick V. Brady	Org. 6730
1	MS0771	Stanley A. Orrell	Org. 6800
1	MS0779	Kevin A. McMahon	Org. 6772
1	MS1136	Gary E. Rochau	Org. 6771
1	MS1137	Stephanie P. Kuzio	Org. 6733
1	MS1317	Evaristo J. Bonano	Org. 6780
1	MS1317	Palmer Vaughn	Org. 6782
1	MS1369	Geoff Freeze	Org. 6783
1	MS1369	Robert Mackinnon	Org. 6781
1	MS1369	Peter N. Swift	Org. 6780

1	MS0899	Technical Library	9536 (electronic copy)

For LDRD reports, add:

1	MS0123	D. Chavez, LDRD Office	1011

For CRADA reports add:

1	MS0115	OFA/NFE Agreements	10112

For Patent Caution reports, add:

1	MS0161	Legal Technology Transfer Center	11500


Sandia National Laboratories